UNIVERSITÀ DEGLI STUDI DI PADOVA

Dipartimento di Ingegneria dell'informazione
Corso di laurea magistrale in Bioingegneria

Characterization of printed sensors for monitoring hydration with wearable devices

Master Candidate

Alberto Zacchini

Student ID 2021178

Supervisor

Sarah Tonello

University of Padova

Academic Year and graduation date

2022-2023

February 27, 2023

Co-supervisor

Alessandra Galli

University of Padova

Abstract

Dehydration is a condition that can lead to serious health complications, including death, if not timely compensated, especially in the elderly. The difficulties of verifying hydration status are given by the limitations existing both in terms of monitoring methods and of standardized assessment scale of hydration status. Home hydration monitoring devices could help to prevent such condition, but to date, a fully wearable, low-cost, easy-to-use, and stand-alone medical healthcare device for dehydration monitoring is not yet available. In this thesis, the main focus was the characterization of flexible non-invasive sensors used in a prototype device designed to monitor the hydration status of the human body. Considering a trade off between medical relevant parameters and portability, three sensors were selected: a Resistance Temperature Detector (RTD) sensor to measure body temperature, an interdigitated sensor to monitor local skin hydration through changes in electrical characteristics, and tetra-polar electrodes to monitor global changes in body water content through Bio-Impedance Analysis (BIA). All sensors were characterized first on *In Vitro* models and then in vivo.*In vitro* and *in vivo* obtained results confirm the functionality of the platform. In particular, sensors *in vitro* characterization allowed to confirm the ability of the sensing element to follow changes in the targeted quantities and enables the selection of a single frequency for simplifying measurements with the portable electronics.*In vivo* characterization showed results in agreement with the measurements performed *in vitro*, after an initial time needed to reach the steady state. Preliminary *in vivo* tests performed on two subjects confirmed the possibility of detecting proportional changes in both local and global impedance due to changes in the body's hydration status. Overall, the reported results represent the fundamental proof needed for the development of a fully operating device that can be used satisfactorily in a real application scenario.

Sommario

La disidratazione è una condizione che, se non compensata tempestivamente, può portare a gravi complicazioni per la salute, compresa la morte, soprattutto negli anziani. Le difficoltà nel verificare lo stato di idratazione sono date dalle limitazioni esistenti sia in termini di metodi di monitoraggio che di scala di valutazione standardizzata dello stato di idratazione. I dispositivi di monitoraggio dell'idratazione ad uso domestico potrebbero aiutare a prevenire tale condizione, ma ad oggi non è ancora disponibile un dispositivo medico-sanitario completamente indossabile, a basso costo, facile da usare e autonomo per il monitoraggio della disidratazione. In questa tesi, l'obiettivo principale è stato la caratterizzazione di sensori flessibili non invasivi utilizzati in un prototipo di dispositivo progettato per monitorare lo stato di idratazione del corpo umano. Considerando un compromesso tra parametri di rilevanza medica e portabilità, sono stati selezionati tre sensori: un sensore resistivo di temperatura (RTD) per misurare la temperatura corporea, un sensore interdigitato per monitorare l'idratazione locale della pelle attraverso i cambiamenti delle caratteristiche elettriche e elettrodi tetra-polari per monitorare i cambiamenti globali del contenuto di acqua corporea attraverso l'analisi della bio-impedenza (BIA). Tutti i sensori sono stati caratterizzati prima su modelli *In Vitro* e poi *In vivo*. I risultati ottenuti confermano la funzionalità della piattaforma. In particolare, la caratterizzazione dei sensori *In Vitro* ha permesso di confermare la capacità dell'elemento sensibile di seguire i cambiamenti nelle grandezze desiderate e consente di selezionare una singola frequenza per semplificare le misure con l'elettronica portatile. La caratterizzazione *In Vivo* ha mostrato risultati in accordo con le misure eseguite in vitro, dopo un tempo iniziale necessario per raggiungere lo stato stazionario. I test preliminari eseguiti *In Vivo* su due soggetti hanno confermato la possibilità di rilevare variazioni proporzionali dell'impedenza locale e globale dovute a cambiamenti nello stato di idratazione dell'organismo. Nel complesso, i risultati riportati rappresentano la prova fondamentale necessaria per lo sviluppo di un dispositivo completamente funzionante che possa essere utilizzato in modo soddisfacente in uno scenario applicativo reale.

ACKNOWLEDGEMENTS

I want to thank every person who participated in the enormous journey I took before I got to this point, it was an immense honor to be able to share special moments with all my colleagues and, especially, friends, who supported me all this time, and to my supervisors Sarah Tonello and Alessandra Galli for providing me the opportunity to participate in this project. I would especially like to thank my parents who have always supported me, and for the unconditional affection and love they have had for me from the beginning.

Contents

Chapter 1

BACKGROUND AND MOTIVATION

Body hydration is an important factor that determines the health status of the body, and allows it to regulate many of the physiological functions of the body; as is well known, the body consists of between 55% and 75% water, where the extreme cases are the elderly and children, respectively [1]. Dehydration is a condition of deprivation of sufficient water for the body's regular physiological functions, caused by inadequate diet, intake of medications (especially diuretics or laxatives) or excessive fluid loss resulting from a pathological condition (vomiting, diarrhea, diabetes and other conditions).

In elderly patients, inadequate water intake can be extremely risky, because the consequences associated with dehydration can lead to a rapid decline in organ function, an absence of sweating that causes a rise in temperature (up to 42 °C), an acceleration of the heart rate that can lead the patient to a severe condition [1].

The development of a device that allows the most accurate and rapid detection of an elderly patient's hydration condition is of fundamental importance to maintain a balance of physiological functions and patient well-being.

The proposed hydration status assessment device is designed to be extremely accurate, thanks to the presence of three specific sensors that allow different types of measurements, where the union of the measurements will allow to accurately define the condition of the patient. This thesis envisages designing and developing a prototype of a multisensing device that can evaluate and monitor the hydration status of a subject. In this thesis, in Chapter 2 is explained how hydration state affects normal biological functions, highlighting the pathological aspects that dehydration can bring. The state of the art of current devices for evaluating hydration is also reported. The third chapter is dedicated to the design and fabrication of the sensors that make up the device, detailing the printing process, the materials used, and the geometry of each sensor. The fifth, sixth and seventh chapters describe all the tests, including individual *In Vitro* tests for each sensor, and finally, *In Vivo* characteriza-

tion and *In Vivo* tests with the complete device. The choices regarding the protocol for data acquisition will be thoroughly explained. Finally, the last chapter will be devoted to conclusions, the results of the project and future research to improve the functionality and accuracy of the device.

Chapter 2

HYDRATION STATUS AND TRADITIONAL ASSESSMENT STRATEGIES

This chapter aims to describe the physiology of water in the human body, emphasizing the main issues caused by the state of hydration. In addition, the state of the art of devices that measure hydration, especially those that exploit Bio-Impedance Analysis and those that measure the local hydration state of the skin, but also new developments and research that aim at a precise and noninvasive measurement of hydration status are reported.

2.1 Water physiology

Under physiological conditions, the human body is composed of approximately 70% water, which is distributed among the so called water compartments, that are separated by selectively permeable membranes and differ in their chemical composition. The main compartments are 65% intracellular fluid (ICF) and 35% extracellular fluid (ECF), which includes tissue or interstitial fluids, blood plasma, and lymph, as well as transcellular fluids [2]. Fluids move from one compartment to another via capillaries and plasma membranes. Through osmosis, water is transferred from the digestive tract to the bloodstream and through capillary filtration, it passes from the blood to the interstitial fluid. The water found in the interstitial fluid can be reabsorbed by the capillaries or carried away by the lymphatic system, which returns it to the circulatory bloodstream [2].

Dehydration is the most common form of water imbalance (other forms are fluid excess and fluid sequestration) and can be defined as a negative water balance: the amount of fluid intake is less than what is excreted. Fluid loss can be the cause of complex pathological case. The pathological conditions that dehydration can cause are many, such as [1]:

- heat injury, varying in severity from mild heat cramps to heat exhaustion or life-threatening heat stroke;
- urinary and kidney problems. Prolonged or repeated bouts of dehydration can cause urinary tract infections, kidney stones and even kidney failure;
- out-of-balance electrolytes, such as potassium and sodium, can cause normal electrical messages to be garbled, resulting in involuntary muscle contractions and seizures.
- low blood volume shock (hypovolemic shock). This is one of the most serious, and sometimes life-threatening, complications of dehydration and it occurs when low blood volume causes a drop in blood pressure and a decrease in the amount of oxygen in the body.

It is therefore of utmost importance to keep the amount of water in the body within physiological ranges for homeostatic balance and to avoid any kind of pathological condition that could, in extremes, become fatal.

The "gold standard" methods for measuring the amount of fluid in the human body are based on isotope dilution, total body potassium (TBK), γ-ray emission measurement and sodium bromide (NaBr) dilution, respectively, for measuring total body water (TBW, "Total Body Water"), intracellular water (ICW, "Intracellular Water") and extracellular water (ECW, "Extracellular Water"). However, methods for estimating TBW based on different modes of bioimpedance analysis (BIA, "Bioimpedance Analysis") are becoming increasingly popular [26]. These are indirect, non-invasive methods that are faster and easier to use than their predecessors. Other parameters are then investigated that may be efficient for monitoring hydration status, such as local skin hydration, which is measured with special sensors discussed in the following sections.

2.2 Parameters affected by hydration status

Water intake must be maintained at levels to ensure all the functions in which it participates. In general, there are two major compartments into which we can divide the water present in the human body: intracellular water and extracellular water. The regulation of both is necessary for survival and occurs through a mechanism of homeostasis, maintained by the concentration of ions present in the water in the two compartments [19].

Generally, the need for water is signaled to the brain due to homeostasis, which causes the person's thirst stimulus. However, the thirst stimulus is confusing, precisely because there is a constant introduction of fluids throughout the day, and often water is also introduced for reasons unrelated to thirst, as in the case of food, where

the primary goal is the feeding; moreover, it is reported in the literature how the mechanism of thirst signaling decreases with increasing age, causing forgetfulness in the intake of sufficient water intake in the elderly [20].

Some condition that are affected by water are related to a person's physical and mental condition. In the physical, in the presence of relatively mild levels of dehydration, individuals engaging in physical activity experience decreased performance related to reduced endurance, increased fatigue, altered thermoregulatory capacity, reduced motivation, and increased perceived exertion [21]. Similar to physical functioning, small and medium amounts of dehydration can affect performance in short-term memory, perceptual discrimination, arithmetic ability, visual-motor tracking, and psychomotor skills. This phenomenon does not always seem to occur at the same state of dehydration but varies among individuals [22][23].

There are quantifiable parameters closely related to a person's water and hydration status, and they are of utmost importance to the patient's health status. One of these very important parameters is blood volume, which is closely related to blood pressure and heart rate. One of the aspects that must be maintained in the blood to maintain its optimal volume levels is plasma Osmolality, which must be kept in the ranges of 275-290 mOsm/kg. Its regulation is kept constant by the kidneys, which through osmoreceptor and baroreceptor cells, are able to stimulate the release of vasopressin, maintaining water retention and increasing urine concentration [24]. Closely related to plasma osmolality, urine osmolality, used as a method of assessing hydration status, normally ranges from 40 mOsm/kg to a maximum of 1400 mOsm/kg [24]. The other two related parameters are blood pressure and heart rate. A direct increase in the amount of water causes an increase in blood pressure and a decrease in heart rate, both of which are influenced by the increase in blood volume and the response to the increase in volume by vasoconstrictor sympathetic activity [25].

2.3 Gold standard monitoring techniques

Measuring hydration status is a challenge because of the constant fluctuations and complex fluid-regulation dynamics of the body. Several techniques have been studied and are considered Gold Standard for hydration status assessment; below are the absolute most widely used techniques with their pros and cons.

One of the most accurate methods for estimating water in the body is the use of isotope tracers. An isotopic tracer is a unique, radioactive or enriched, uncommonly stable isotope of the element to be traced to allow subsequent determination of its distribution or location. Their size allows them to enter through the compartments of the body and become tracers in the districts, allowing an analysis of the amount of water. This method uses different types of tracers to assess Total Body Water

(TBW), and extracellular (ECV) and intracellular (ICV) fluid compartments [26]. The formula used to estimate the amount of fluid is:

$$PV_1XPC_1 = PV_2XPC_2 \tag{2.1}$$

Where PV_1 and PC_1 are plasma volume and plasma concentration before tracers intake and PV_2 and PC_2 are plasma volume and plasma concentration after 3/4 hours of tracers intake [27]. There are numerous types of isotopes that are used, due to their different characteristics, such as deuterium ^2H, deuterium oxide ^2H_2O, and oxygen-18 ^{18}O. Bromides are also used because they are partially soluble in water but very soluble in organic solvents. However, this technique has some cons, starting with the complexity of isotope analysis, which requires sophisticated clinical equipment and experienced laboratory staff, increasing the time of and costs. In addition, the use of radioactive tracers it's not harmful but does not allow immediate repeatability of the experiment.

Another widely used method for the assessment of hydration status is the use of the Neutron activation analysis (NAA) method. The method consists of exposing a subject to low doses of irradiation that causes the production of radionuclides, where they will emit characteristic rays during decay [30], and where their decay pathway has been previously assessed, and it is then possible to trace the amount of water present. It is an extremely accurate method, but again the high costs due to the needed specialized staff and laboratory and the non-repeatability of the test because of radiation [30], make the method difficult to use.

Many hematological parameters have been used for the assessment of hydration status, blood testing being easy to perform and available in all clinical facilities. The most widely used blood parameter is plasma osmolality (concentration of solutes in the blood). Osmolality is calculated through the formula [29]:

$$BloodOsmolality = 2(Na\frac{mmol}{L}) + (K\frac{mmol}{L}) + Glucose(\frac{mmol}{L}) + Urea(mmol/L) \tag{2.2}$$

According to the literature reports, a level greater than the value of 300 mOsm/kg is considered a state of clinical dehydration [32], while a value of about 295 mOsm/kg is considered mild dehydration [28]. Another important marker that is used for hydration assessment by blood tests is Blood Urea Nitrogen (BUN), combined with creatinine assessment. A BUN of about 6.7 mmol/L and a creatinine concentration of 150 μmol/L might suggest an imbalance of fluid or electrolytes [29]. Normally, BUN and creatinine are measured together with packed cell volume (PCV), also known as the volume of red blood cells in the blood. Normal values are 0.54L/L in men and 0.47L/L in women [29].

Other techniques widely used for hydration assessment are based on two param-

eters that describe the patient's urine. The first is urine osmolality, which is the concentration of solutes in the urine. Urine osmolality is the best method for indicating solute concentration and describing kidney concentrating abilities [31], but less useful for assessing hydration status. The calculation for urine osmolality is [29]:

$$UrineOsmolality = 2(Na\frac{mmol}{L}) + K\frac{mmol}{L}) + Urea(mmol/L) \tag{2.3}$$

Urine specific gravity (SG) relates to the concentration of solutes and is presented as a ratio of the weight of the urine to the weight of an equal amount of water. SG of distilled water equals 1 and the urine values above 1.025 indicate concentrated urine that may be a result of dehydration [29]. SG over 1.020 indicates mild or impending dehydration.

Chapter 3

NON-INVASIVE SENSING DEVICES FOR HYDRATION MONITORING

Multi-sensor medical devices are instruments that use multiple sensors to collect and analyze an individual's biometric data. These devices are often used to monitor vital parameters such as heart rate, blood pressure, and blood oxygen level. In addition, they can be used to detect signs of chronic diseases such as diabetes and sleep apnea. Multi-sensor medical devices can be worn as portable devices or integrated into other medical products such as beds or wheelchairs. They are particularly useful for remote monitoring of patients because they can send the collected data to a physician or other health professional in real time. One of the advantages of multi-sensor medical devices is their ability to collect and analyze a wide range of biometric data.. The characteristic of being "noninvasive" comes from the ability to measure biological parameters without entering the body. The main categories of noninvasive sensors are divided mainly into electrodes that assess impedance , biosensors for sweat analysis, and sensors for physiological parameters (temperature, ECG and many others). Combining the capabilities of multisensor and noninvasiveness can be a real game-changer in assessing the health status of patients, decreasing the risk of harm given by invasive techniques, and ensuring effective assessment given by the analysis of multiple parameters.

An example of a multi-sensing device is the smart contact lens that assesses blood glucose by reading biomarkers in tears. Specifically, in the work done by Joohee Kim et al. [51], they have developed a lens that can read multiple biomarkers from tears and simultaneously measure intraocular pressure, through the use of a sandwich structure composed of the spiral structures of graphene(to measure glucose) where a layer of Ecoflex(to measure intraocular pressure) was inserted in between.

Another work done by Pham et al. [52] is to develop a multi-sensing device that can assess heart rate, oxygen saturation, physical activity levels, skin temper-

ature, and galvanic skin response. To monitor all these parameters, a temperature(infrared) sensor, a pulse oximeter sensor, an accelerometer, and a skin galvanic response sensor were incorporated into the device, all connected to a microcontroller.

Other multisensing device developed by Sempionatto et al. [56] consists of a patch that analyzes interstitial fluid glucose and other biomarkers such as lactate, caffeine, and alcohol in sweat, while also capturing physiological changes involved in different food intake(e.g., blood pressure and heart rate). The patch is composed of a number of separate enzymatic chemical sensors that analyze interstitial fluid and sweat, while they have a sensing structure consisting of a two sensors for iontophoresis and an acoustic system for the detection of alter echoes.

In this section, a comprehensive description of the components comprising the hydration monitoring device is provided. The device consists of three key components: a serpentine resistance temperature detector (RTD) for temperature measurement, an interdigital sensor for the assessment of local hydration status through resistance measurement, and (3) a 4-wires configuration for bio-impedance analysis. The combination of these components enables the device to accurately measure and evaluate the hydration levels of the body.

3.1 Bio Impedance Analysis

Bio-impedance analysis is a noninvasive and rapid method for evaluating the electrical characteristics of biological tissue. The electrical properties of tissue are closely related to the characteristics of the extracellular fluid, cell membrane and intracellular fluid [10]. There are a variety of methods applied for interpretation of measured bioimpedance data and a wide range of utilizations of bioimpedance in body composition estimation and evaluation of clinical status. The electrical properties of biological tissues are currently categorized based on the source of the electricity, i.e., active and passive response. Active response occurs when biological tissue provokes electricity from ionic activities inside cells, like signals from the heart and electroencephalograph signals from the brain. Passive response occurs when biological tissues are simulated through an external electrical current source. Bioimpedance or biological impedance is defined as the ability of biological tissue to impede electric current and is considered as a passive response [10][11].

Bioimpedance is a complex quantity composed of resistance (R) which is caused by total body water and reactance (Xc) that is caused by the capacitance of the cell membrane:

$$Z = R + jX_c \tag{3.1}$$

$$R_{(\Omega)} = \rho_{(\Omega m)} \frac{L_{(m)}}{A_{(m^2)}} \tag{3.2}$$

$$X_{c(\Omega)} = \frac{1}{2\pi f_{(Hz)} C_{(Farad)}} \tag{3.3}$$

The resistance of an object is determined by its shape, described by its length (L) and surface area (A), and the type of material, described by its resistivity (ρ), as shown in equation 3.1 [10] [12].

The reactance (Xc) of an object is defined as the resistance to voltage change across the object and is inversely related to signal frequency (f) and capacitance (C). In biological systems, resistance is caused by the total water flowing through the body, while reactance occurs due to the capacitance of the cell membrane.

Capacitance (C) is defined as the capacity of a nonconducting object to store electrical charges, equal to the ratio of the voltage differential across the object (dV/dt) to the current flowing through the object (I(t)).

Through these values, special formulas have been created that are based on the values of impedance, age, sex and weight, which allow calculation of the main values such as FFM (Free Fat Mass), or lean mass, FM (Fat Mass), or body fat, and finally TTW(Total Body Water), the amount of body fluid expressed as a percentage.

Several BIA techniques have been developed:

- Analysis of bioimpedance information obtained at 50 KHz electric current is known as single-frequency bioimpedance analysis (SF-BIA). SF-BIA is the most used and is one of the earliest proposed methods for the estimation of body compartments. It is based on the inverse proportion between assessed impedance and TBW, which represents the conductive path of the electric current. SF-BIA predicts the volume of TBW that is composed of fluctuating percentages of extra cellular fluid (ECF) which is almost equal to 75% of TBW, and ICF that represents the rest. SF-BIA instruments have been used to assess TBW and FFM using the derived Equations.

- MF-BIA (Multifrequency-BIA) is based on finding ECF and TBW through exposition of the body to low and high frequency electric currents, respectively. In general, the MF-BIA method predicts ECF more precisely than the SF-BIA method; however, in elderly diseased subjects, the MF-BIA method shows less sensitivity in detecting fluid shifts between ECF and ICF [13].

- Analysis of bioimpedance data obtained using a broad band of frequencies is known as bioimpedance spectroscopy (BIS). The BIS method is based on the determination of resistance at zero frequency (R0) and resistance at infinity frequency (Rinf) that is then used to predict ECF and TBW, respectively.

Bioimpedance is measured through the use of 4 electrodes where 2 are used for injection and detection of alternating current and 2 are instead used for voltage measurement. There are different types of measurement including hand-foot, foot-foot, hand-hand method.

Some examples of devices used in clinic rooms are the Tanita® and the SECA® 525 Medical Body Composition Analyzer(fig.3.1), which is capable of estimating the amount of fat, water, muscle and other body parameters of a subject lying on the device's measurement mat, and is very accurate because it uses a hand-foot measurement on both sides of the body.

There are also miniaturized devices designed to perform such measurements, such as the IBIS multifrequency bioimpedance monitoring unit, developed at the Holst Centre and based on the MUSEIC multi-parameter on-chip acquisition system(fig.3.2). This device was used to study physiological stress under stress related to dehydration.

Figure 3.1: SECA 525 Medical Body Composition Analyzer

Another experimental approach, very similar to Bioimpedance Analysis, for assessing hydration status using microwaves was developed by Deepesh Agarwal et al. [15]. The study reports an analysis of changes in attenuation coefficient between a pair of planar antennas placed on a subject's arm during various hydration states, evaluating changes in electromagnetic attenuation coefficient in the frequency range 2-3.5 GHz over 30 minutes during periods of heat stress (hypohydration), rest (con-

Figure 3.2: Holst Centre IBIS mutltifrequency bioimpedance monitoring unit

trol euhydration) or recovery after heat stress (rehydration). The corresponding study [15] demonstrates the ability to predict acute changes of <2% in whole-body hydration(fig.3.3).

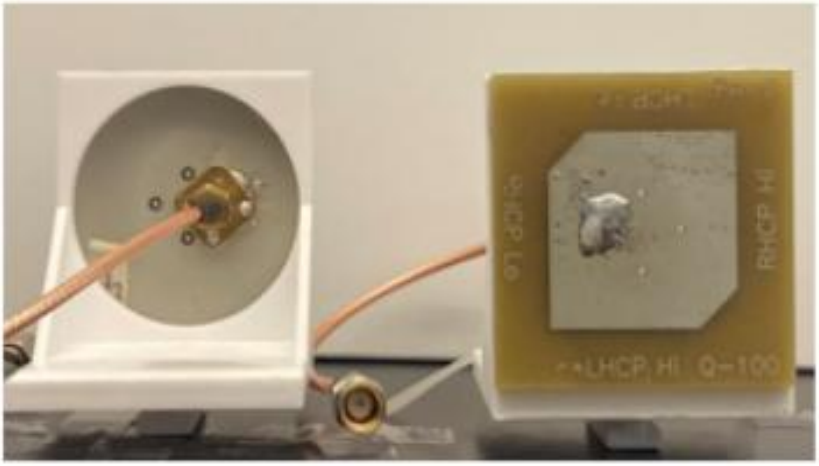

Figure 3.3: Antennas for hydration assessment

3.2 Skin hydration

Skin hydration is an important factor in maintaining healthy skin. When the skin is well-hydrated, it looks plump and glowing, and is better able to protect itself from the elements. Dehydrated skin, on the other hand, can appear dull and lifeless, and is more prone to irritation and damage. There are several factors that can lead to dehydrated skin, including exposure to the sun, wind, and cold weather, as well as hot showers, air conditioning, and other environmental factors. In addition, certain medical conditions, such as diabetes and eczema, can also cause the skin to become dehydrated. Checking for proper skin hydration is essential to assessing a person's overall hydration status, which is why research is investigating solutions for measuring hydration status in the skin through the use of sensors.

S. Yao, A. Myers et al. [14] proposed a sensor, capable of being in close contact with the skin, that provides continuous monitoring of its hydration status based on impedance measurement. More specifically, the device under consideration includes stretchable, interdigitated electrodes. They are made using silver nanowires (Ag-NWs, "Ag Nanowires"), embedded below a layer of polydimethylsiloxane (PDMS). The nanowires form interdigitated patterns, which are critical for maximizing the interaction between electrodes in a small space. Contact pads are used to connect hydration sensors to other circuit components. Due to the high conductivity of silver and the mechanical strength of polymers and nanomaterials, the device overall has good conductivity.

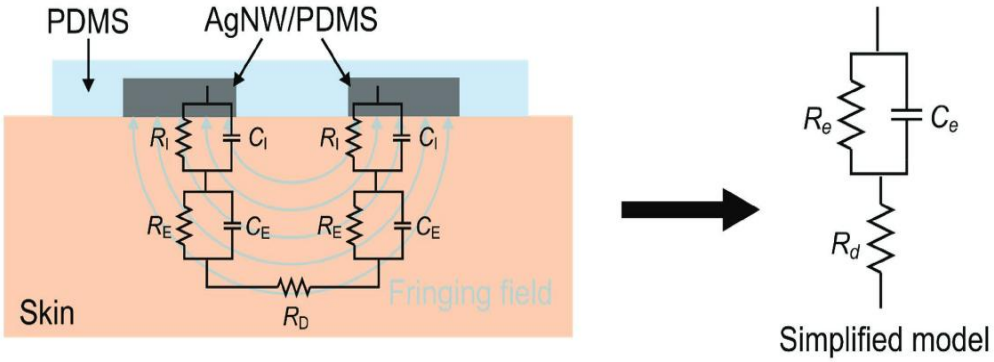

Figure 3.4: Interdigitate skin hydration sensor [14]

The skin impedance measurement required for estimating the hydration state is made possible by the two electrodes that make up the sensor and can be modeled electrically by resorting, as usual, to capacitance and resistance. Specifically, the electrode-skin interface can be described by the parallel between the resistance RI and the capacitance CI, the epidermis by the parallel between the resistance RE and the capacitance CE, and the dermis by the resistance RD. Given the symmetry of the electrodes, the electrical equivalent just described can actually be seen as the parallel between resistance Re and capacitance Ce, both arising from the electrode-skin interface and from the epidermis, connected in series with the resistance Rd, related to the dermis and the tissue underneath.

This sensor at present has no application on any kind of commercial device but is expected to be rapidly diffused given its easy production, low cost of materials and an impedance variation discriminating the moisture status of the skin

Another wearable skin hydration sensor based on cotton fabric to determine skin hydration status through impedance analysis was studied by Minju Jang et al. [33]. The sensor structure includes a textile substrate, a thermoplastic overlayer, conductive patterns, and an encapsulant, designed for stable and reliable monitoring of skin impedance change in relation to hydration level [33]. Cotton textile substrate was cut into a rectangular piece of 10 cm × 10 cm. A thermoplastic polyurethane (TPU) film with a thickness of 50 µm was placed, followed by Ag paste and encapsulant.

Afterward, it was stored at room temperature for at least one week to achieve the best adhesiveness and detection performance.

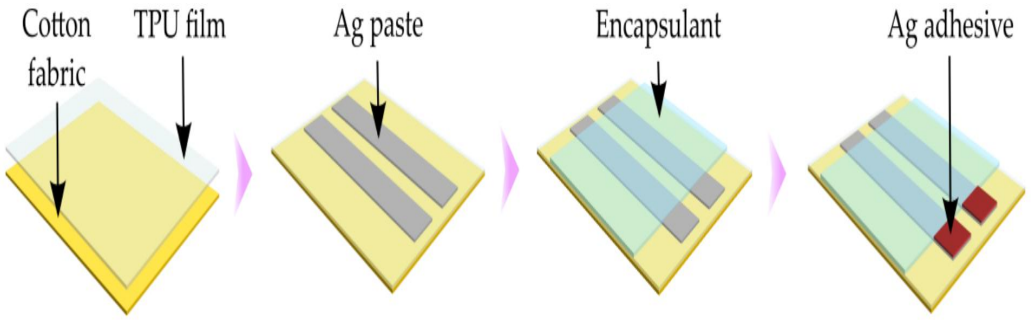

Figure 3.5: Textile-based sensor fabrication

Both the characteristics of sensor geometry and the frequency of the current chosen for the test impact the depth of the electric field created by the sensor. For this reason, the width of the electrodes was chosen to be 5mm, while the frequency used for the test was in the range of 1 Hz-100 KHz.

3.3 Sweat analysis: rate and ion quantification

Sweat contains a great deal of biochemical information that can reflect the state of the organism at the molecular level. There are two categories of stimulation of sweat production: passive and active. Passive stimulation often occurs due to hot or humid weather and serves to maintain normal body temperature by evaporating sweat to decrease body heat. Sweat resulting from active movement is called active sweating and not only sustains normal body temperature, but also carries away a small amount of waste products generated by the body during exercise [9].

Several studies reveal a potential interest in the ion balance (especially sodium and potassium) of sweat as a predictive biomarker of dehydration when combined with the amount of sweat and information from other sensors. The quantification can be easily achieved by using an arrangement of 2 electrodes, performing an open-circuit potentiometric measurement [5].

Sweat is an analyte-rich fluid secreted by sweat glands on human skin and plays an important role in thermoregulation of the body. Sweat glands can be classified into two categories: eccrine and apocrine. Eccrine glands are the most considered in the case of sweat analysis, because apocrine glands are present in areas in close contact with hair or scalp, creating a sweat rich in proteins and lipids, making sweat analysis more difficult [34]. There are two very important aspects that characterize sweat, aspects that can then be used to assess a person's health and hydration status. The two aspects considered are sweat rate and sweat composition. Sweat production is controlled by central and peripheral control; the former, managed by

the hypothalamus, centrally controls sweat rate, influencing the frequency of expulsion, while peripheral control takes charge of aspects of the glands, such as the amount of sweat expelled during expulsion [35]. Multiple factors can influence central and peripheral control to change sweat rate; the dominant factor for the rise and fall of sweat is body temperature: the higher the body temperature, the higher the pulsatory rate of sweat glands will rise, increasing sweat rate and thus dissipation [36]. Other factors such as an abnormal carbon dioxide level in the blood, where its increase causes an upregulation of sweat rate, while a decrease causes the opposite [37]. Sweat has a varied composition: it contains electrolytes, traces of some metals, cytokines and organic components. It is still unclear why some components are contained in sweat, but electrolytes make up most of the sweat component and are sweat rate dependent. The electrolytes present in sweat are: Sodium (Na+) and Chloride (Cl-), the main indicators of the state of dehydration; Ammonium (NH4+), Potassium (K+), and Calcium (Ca2+) [38]. The techniques for measuring sweat rate parameters and ion composition are different, and are distinguished in the two stages of sweat assessment: collection techniques and composition analysis techniques. Collection techniques are used to collect sweat (from eccrine glands) for subsequent analysis of analytes. We first have the microfluidic technique, which is the most widely used in sweat analysis devices: it involves the use of collectors with microfluidic characteristics that take advantage of capillarity to make the sweat reach the interior of the device. However, this does not allow for rapid analysis and only works well at high sweat rates [39]. Another technique is absorption, using an absorbent material that is applied between the skin and the analysis device to collect sweat. The disadvantage is the time resolution and averaging that can only be done over large volumes of sweat, being that the analysis is done only when the absorbent material is saturated with sweat [39]. Last technique, on the other hand, is direct skin contact, allowing rapid analysis without a sweat collection mechanism [39]. Sweat component analysis techniques are numerous, but they fall into two macrocategories: electroanalytical, that is, exploiting a potential difference due to the presence of electrodes, and optical. Electroanalytical techniques are numerous and are extremely effective in measuring the presence of electrolytes and metals in particular. We have firstly the Potentiometric measurement, which measures the potential between two electrodes, and is very useful for assessing pH and electrolyte concentration, making a very rapid detection with minimal use of materials. It also allows the analysis of specific ions through the use of ion-specific electrodes, but it cannot measure the presence of metabolites [40]. Voltammetric measurement allows scanning across electrodes, one analysis electrode and one reference electrode, allowing the extraction of concentrations of multiple analytes. Electrochemical impedance measurement uses a sinusoidal electrical potential, and the reflected wave is then analyzed to measure an analyte. Finally, for electroanalytical measurement we also

have piezo-electric measurement, which is less widely used but does not use external energy suppliers. Optical techniques use colorimetry and fluorometry instead. There are two types of sweat sensing devices: - non-continuous flow, which is a device that has no sweat outlet, cannot do real-time analysis and is dedicated to a single sweat collection for its analysis; - continuos flow, allows dynamic sweat analysis and also allows real-time analysis. Sensors that assess sweat must possess a high level of stability, both because they must maintain their stability during movement and because contact of the sensor with the skin causes artifacts that could significantly reduce the accuracy of the sensor. The current state of the art in sensors has developed sensors that consist of two layers: a solid layer (SC), which functions as an ion-to-electrode transducer, and an ion-selective layer (ISM), which functions as an ion recognizer [41]. The most widely used materials are PEDOT [42], PANI [43], Prussian Blue [44], ChPBN [45], and POT [46]. The most widely used at present is PEDOT, which is then coated with different coatings for the analysis of numerous sweat biomakers, while PANI is widely used for more precise analysis of pH [47].

3.4 Temperature sensors

The body's state of hydration is necessary to maintain an optimal body temperature: the state of dehydration can lead to a thermoregulation problem that can cause the body temperature to rise as high as 42°C in severe cases. Normally, temperature sensors are distinguished according to how they measure heat: there are sensors that measure heat in contact with the surface to be measured, or sensors that measure temperature radiated from the surface, without contact with it.

Temperature sensors are classified as follows: Thermocouples, RTDs (resistance temperature detectors), thermistors, and semiconductor ICs.

Temperature sensors come in various shapes, but the one most commonly used is the typical serpentine shape, which greatly increases the sensing area and allows for high sensitivity with a small surface area [4], and was therefore used for this prototype.

Thermocouples are very high-performance temperature measurement devices that can measure from -270 to about 3000 °C. This type of sensor consists of two dissimilar metal wires joined at one end, connected to an instrument that can accept the input of a thermocouple and measure its reading. They are used because of their low cost, simplicity, robustness and small size. Thermocouples are made of noble metals, base metals, refractory metals and nonmetals [48].

RTDs and thermistors are used in many applications, given their quick response, stability, and ease of insertion on portable and flexible devices, which is why we are going to report more precisely on how these work. Thermistors and RTDs are part of the resistance temperature meters. The resistance of a conductor is directly related

to temperature because the motion of free electrons is temperature-dependent. The RTD sensor is based on the change in the resistance value of the material used during the temperature change. Generally, RTD sensors are constructed based on some standardized curves and tolerance.

Thermistors are similar to RTDs, and consist of sensors made of semiconductor materials(normally a mix of cobalt, magnesium, titanium, and others), where their resistance changes with temperature. Unlike RTDs, the resistance can change either positively or negatively. Another feature is that the formula defining the thermistor's temperature change is nonlinear, so it is necessary to couple two thermistors to partially eliminate the nonlinearity. The advantage of thermistors is that they are very simple and inexpensive [50].

Chapter 4

FABRICATION OF THE MULTI-SENSING PRINTED BRACELET

In this section, the structure and operation of the device is reported, paying particular attention to what are the physical characteristics of each individual sensor inside and their shape , method of production, and choice of material that make them up. The use of multiple sensors serves to ensure a multi-parameter approach and guarantee high accuracy for the detection of hydration status.

The choice of the specific sensors used was related to a trade-off between: 1) quantities of medical interest 2) miniaturizable, easy-to-use, and stable sensors. Ion sensors, although potentially very useful, are still under development for on-body use and present many challenges related to stability and selectivity, having to be functionalized with bioselective membranes. It was preferred to focus more on electrodes that did not require functionalization, thus characterized by greater stability and less complexity.

The sensors that have been used can be distinguished into: Bio Impedance Analysis (BIA) electrodes, used to measure body composition; temperature sensor, useful for detecting changes in body temperature, excellent for assessing an increase in skin surface temperature due to a state of improper hydration; skin hydration sensor, which allow to assess the state of local surface hydration..

All sensors were tested in *In Vitro* models using set ups optimized for each type of sensor, and then studied *In Vivo* to verify the validity of the *In Vitro* data and to confirm their effectiveness.

4.1 Fabrication of printed sensors

Inkjet printing technology, through the Dimatix DMP 2850 printer (FUJIFILM Dimatix, Inc., Santa Clara, California (USA)), was used to create the sensors that

are part of this device. There are two materials that make up each type of sensor and they are:

- printing ink , i.e., a silver ink called Sicrys™ I40DM-106 from PVNanocel ,based on silver crystal nanoparticles in DGME (diethylene glycol monomethyl ether);
- substrate on polyimide sheet (Kapton, Dupont) with a thickness of 50 µm, which possesses excellent thermal, electrical, mechanical and chemical properties, excellent ink adhesion ability during printing and stability after curing [16].

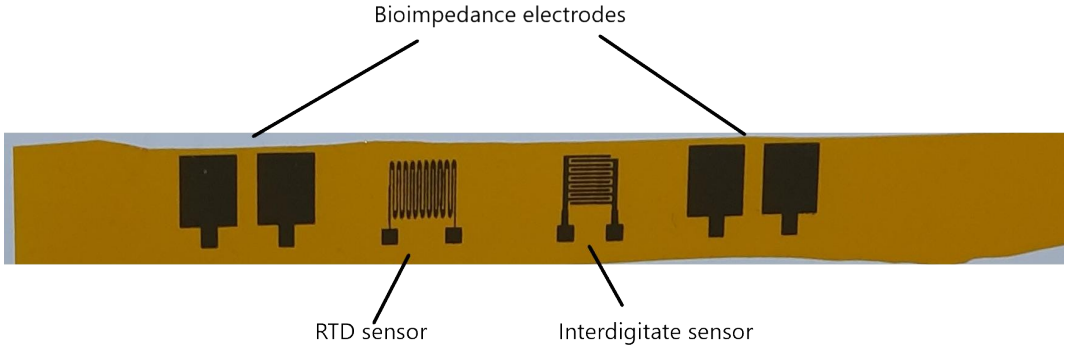

Figure 4.1: Prototype printed sensors

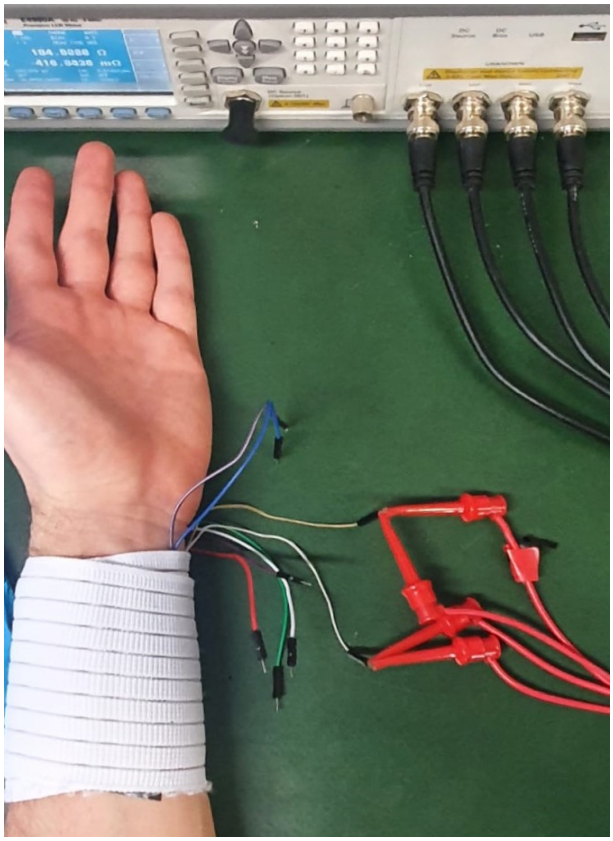

Figure 4.2: Wired prototype attached to the Agilent E4980A LCR Meter for *In Vivo* impedance measurement

4.2 Temperature Sensor

RTD sensor for temperature measurement has been chosen because of its accuracy and precision in varying resistance as temperature changes. Considering that metals are the materials usually suggested from literature to print RTD, a silver nanoparticles based ink was selected in this application. Thus, the nanostructures ensure from one side improved electronic performances, enabling higher sensitivity toward temperature changes, and from the other side optimal chemical stability, ensuring long-lasting durability. Further, the specific nanostructured silver ink selected from PV nanocell is optimized for digital printing, enabling optimal resolution and accuracy in the printed pattern.

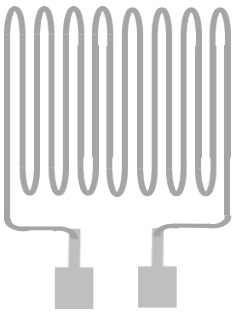

Figure 4.3: RTD sensor with serpentine pattern

Temperature sensor present serpentine shape, which greatly increases the sensing area and allows for high sensitivity with a small surface area [4]. These serpentine patterns are also needed to compensate for the effect of the complementary materials combined with the conductive ink to allow for stretchability, which produces relatively low sensitivities and nonlinearity in the sensor response. In the present device, the temperature sensor was designed exploiting a sensitive surface area of 1 cm^2. In particular, the ink was selected based on previous evidence of work by Barmakos et al. [17], in which it shows a TCR of 0.0027 +- 0.00062 1/°C with printed temperature sensors. After printing and curing RTD at a temperature of 250 °C, two characterization were performed in order to evaluate their suitability. First of all an electrical characterization was performed, measuring the resistance from pad to pad of the serpentine. Values ranging from a minimum of 11.1 Ω and a maximum of 12.4 Ω could be recorded. The average value was of 11.75 +- 0.45 Ω. This correspond to a relative standard deviation of 0.65 Ω.

Figure 4.4: Printed RTD sensor

After that, an optical evaluation of the sensor was performed using an optical microscope and the printer's fiducial camera. The optical evaluation was specifically aimed at verifying that no short circuits were created between the different spaces in the coil, as any connection would have decreased the total resistance and made the sensor less sensitive to temperature changes.

Fig.4.5,4.6 and 4.7 shows some example of the RTD printed acquired with the use of fiducial camera of the Fuji Dimatix printer. As seen in 4.5 and 4.6, the serpentine configuration has a thickness range value from 398 μm to 537 μm. Such a narrow spacing allows for an increase in the number of curves in the serpentine and a larger detection area for the sensor. It is necessary during printing to carefully check the serpentine to avoid overlapping ink phenomena that cause a short between curves,

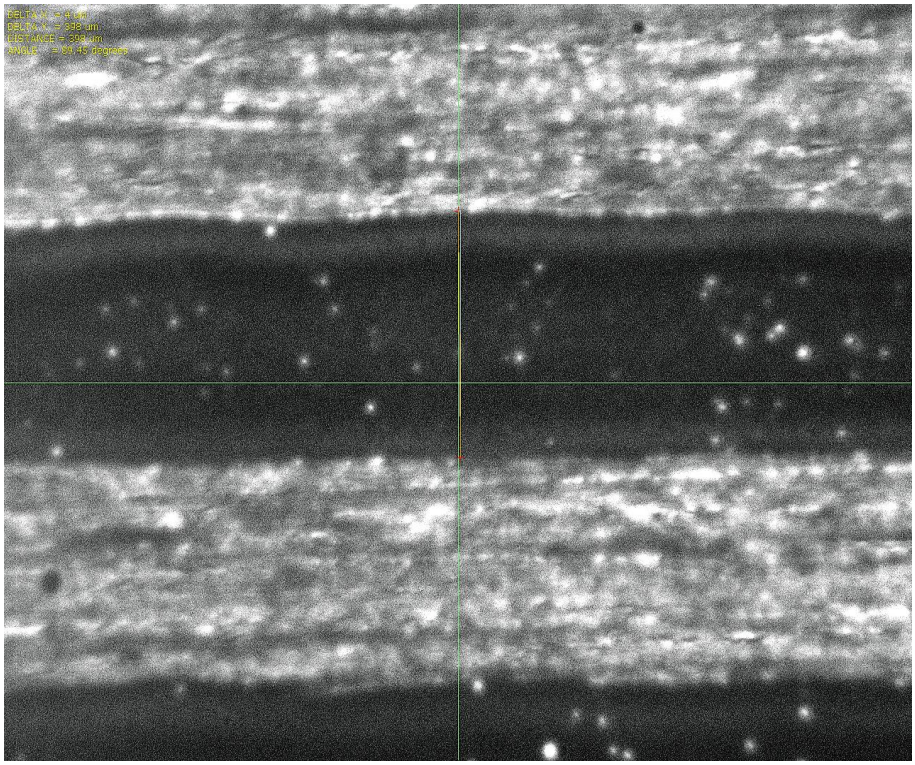

Figure 4.5: Printed RTD sensor serpentine thickness of 398 μm

thus reducing the effectiveness of detection.

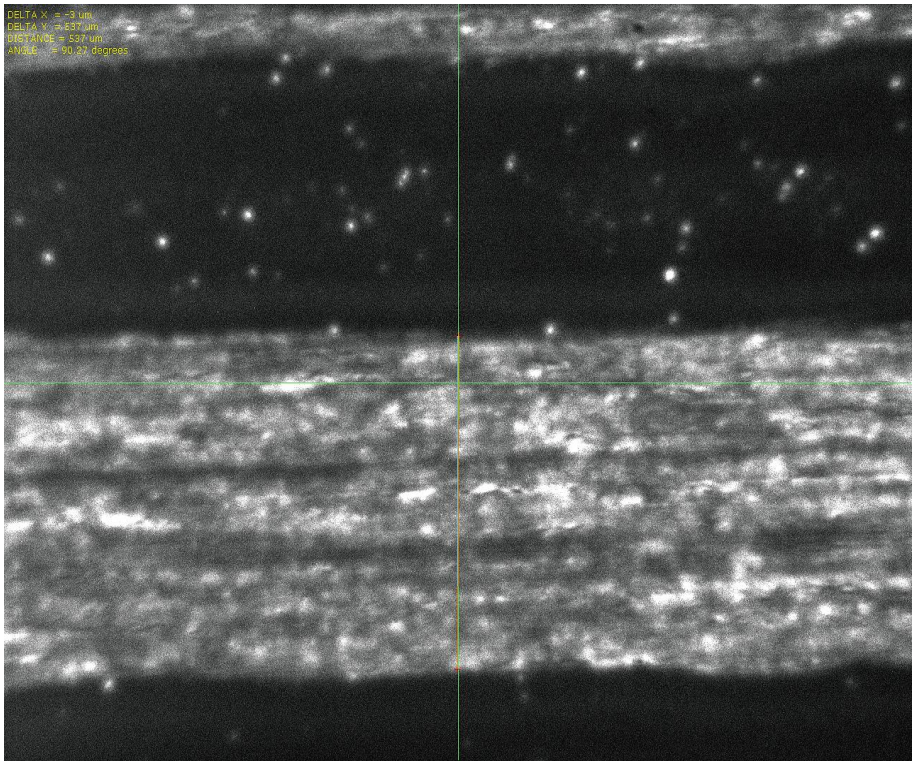

Figure 4.6: Printed RTD sensor serpentine thickness of 537 μm

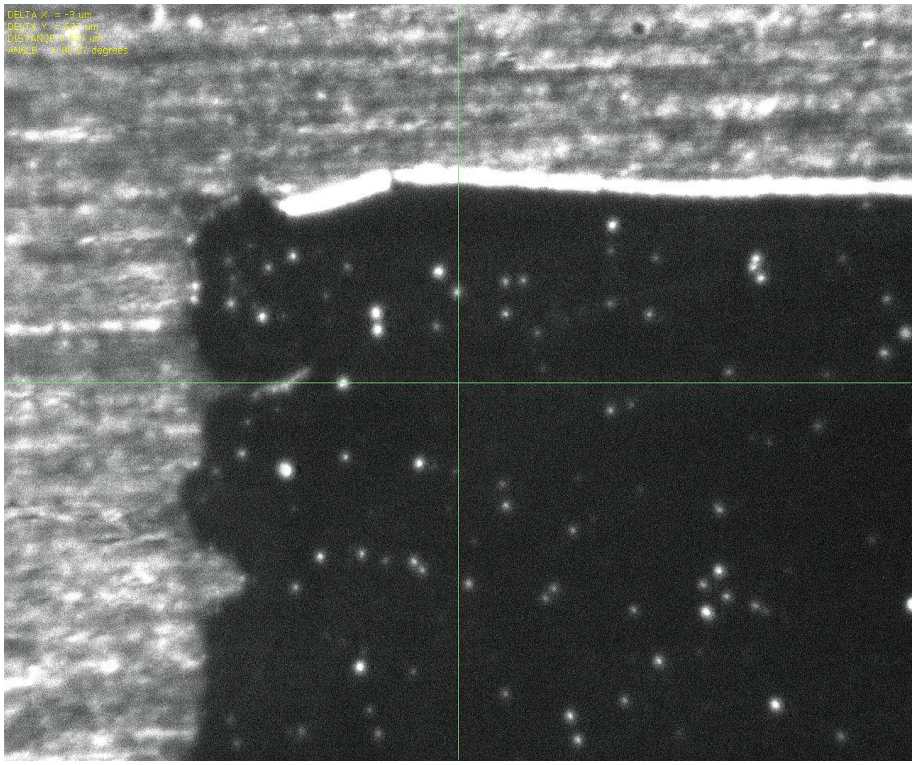

Figure 4.7: Printed RTD sensor pad, used for further cable connection

4.3 Skin Hydration Sensor

As extensively detailed in the background Chapter 3, local skin hydration represent a relevant parameter that might be affected by the overall water balance. The concentration of water in the skin changes the electrical properties of the skin (permittivity and conductivity), and this can be measured through a sensor. The proposed sensor is an interdigitated sensor, which has two unconnected interfaces where the contact surface will allow the circuit to be joined and its conductivity and resistance properties evaluated.

The sensor shape was chosen because it allows for high sensitivity in impedance change during the increase of moisture in the sensing surface [5].

(...)

Figure 4.8: Skin local moisture sensor

These sensors are designed to detect small changes in the electrical properties of the skin, such as dielectric permittivity or electrical conductivity, which vary

depending on the concentration of water in the skin tissues; this detection is accomplished by the small size of the sensor, which consists of an area of 1 cm^2 and an interdigitated shape. Through the use of a simple bench multimeter, it is easy to detect how both sections of the interdigitated sensor exhibit a resistance value that is in the range of 1.1-1.4 Ω, demonstrating its conductivity and functionality

After printing and curing at a temperature of 250 °C, two characterization were performed in order to evaluate their suitability. First of all an electrical characterization was performed, measuring the resistance of both the two part of the interdigitated sensor. Values ranging from a minimum of 1.1 Ω and a maximum of 1.4 Ω could be recorded. The average value was of 1.25 +- 0.02 Ω. This correspond to a relative standard deviation of 0.15 Ω.

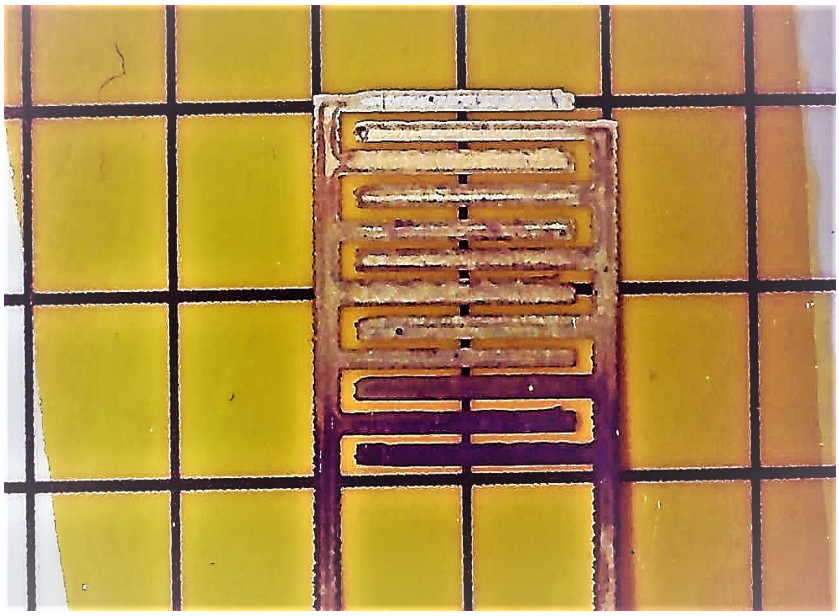

Figure 4.9: Printed skin local moisture sensor

Similar with what was done for the temperature sensor, an optical evaluation of the sensor was performed using an optical microscope and the printer's fiducial camera. The specific purpose of the optical evaluation was to verify that no short-circuit was created between the two parts of the interdigitated sensor, as the injected current would choose the path with lower impedance, that is of the short-circuit itself.

Fig.4.10,4.11 and 4.12, shows details of the interdigitated printed sensor, acquired with the fiducial camera of the Fuji Dimatix printer. As seen in 4.10 and 4.11, the interdigitate electrodes has a thickness range value from 603 μm to 544 μm, that allows for an increase in the number of the electrodes in the sensing area and consequently a larger detection area for the sensor. In4.12,it is possible to see the distance between interdigitated electrodes, with the value of 528 μm.

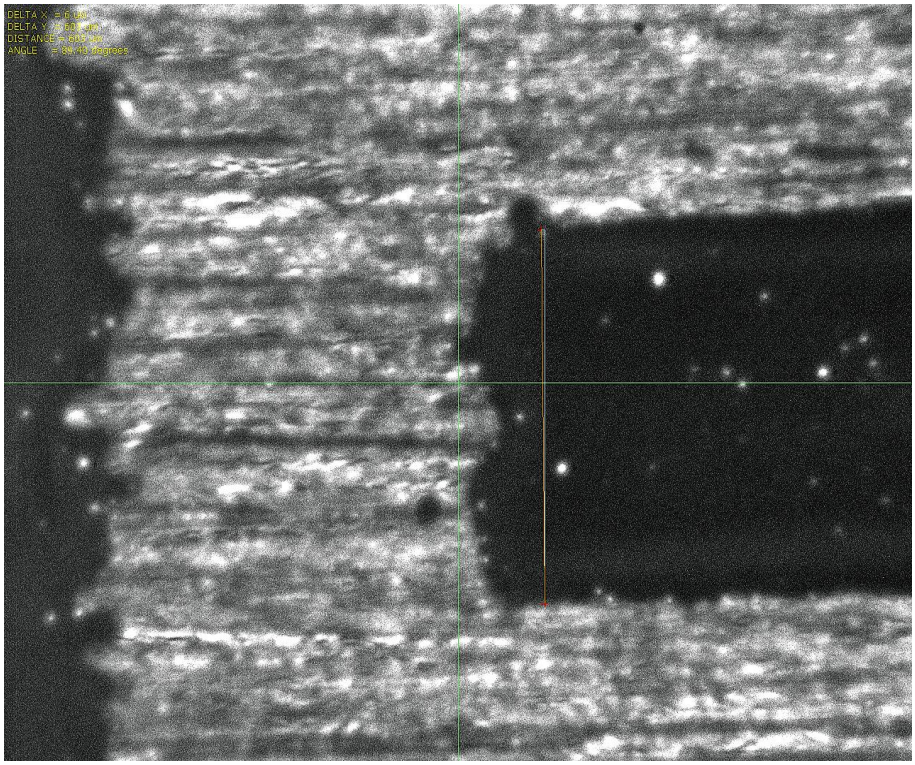

Figure 4.10: Interdigiate electrode thickness(black)

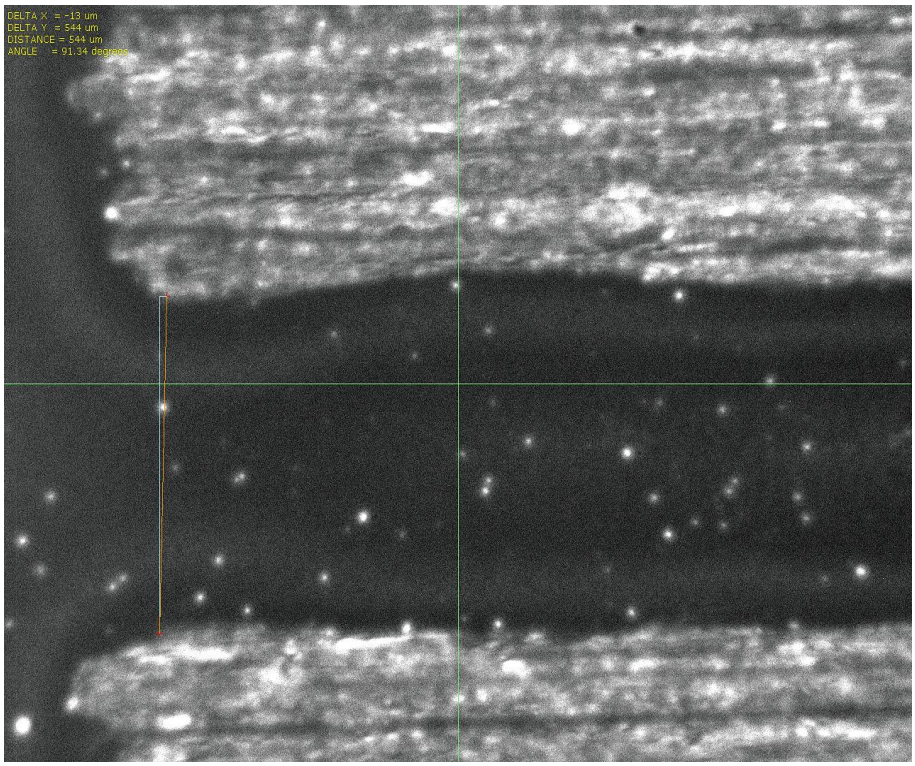

Figure 4.11: Interdigiate electrode thickness(black)

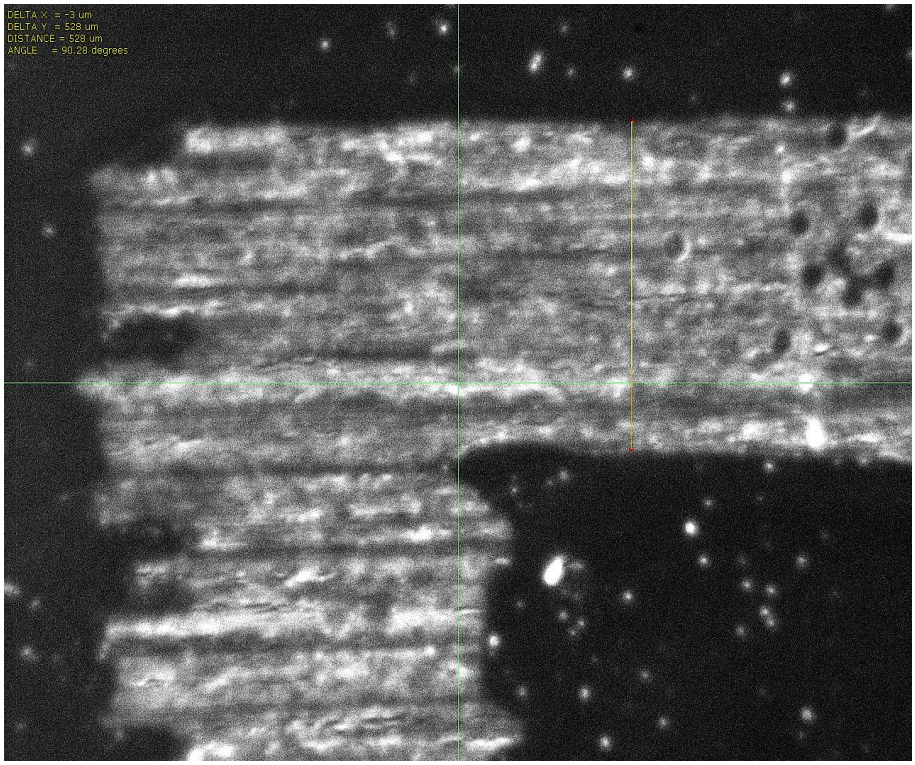

Figure 4.12: Space between interdigitate electrodes (white/gray)

4.4 Bioimpedance Analysis Electrodes

Among the different configuration available from literature to perform BIA analysis (bipolar and tetrapolar) , in this study a tetrapolar configuration was selected. The choice thus ensure higher accuracy and precision in measurements, even with smal sized electrodes.

In this study, the four-electrode configuration(tetrapolar) was chosen as it provides more precise measurements [3]. In this configuration, two electrodes are used to inject a small current into the body to collect impedance data, while the other two electrodes are used to measure the voltage between them. The electrodes are typically placed around the wrist or along the forearm for this type of analysis.

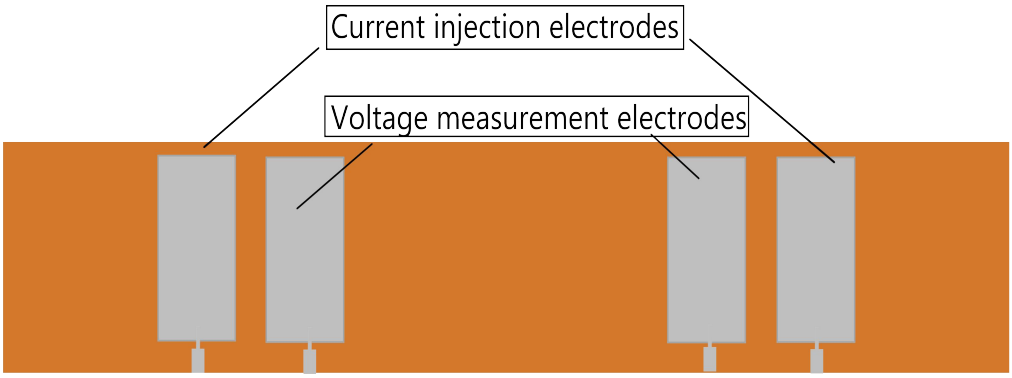

Figure 4.13: BIA four electrodes configuration printed

The electrodes were printed with a silver ink through Dimatix Materials DMP-2850 inkjet printer The size of the electrodes is 1x2 cm, the value of their resistances is between a range of 0.7-1.4 Ω.

In 4.15,4.11 and 4.12, it's possible to see photos of the BIA printed electrodes taken with the Fiducial Camera of the Fuji Dimatix printer. The printing is done accurately , as can be seen from the image, and has a smooth edge, which is essential to maintain the conductivity required for use. A post printing resistance measurement was performed to assess the initial condition of the electrodes before its use in the tests. The resistance values of the measured electrodes are in the range of 800 mΩ-1 Ω. This measurement is crucial because too high resistance would risk preventing a correct reading of the body impedance; in this case, miniaturization does not affect the impedance reading.

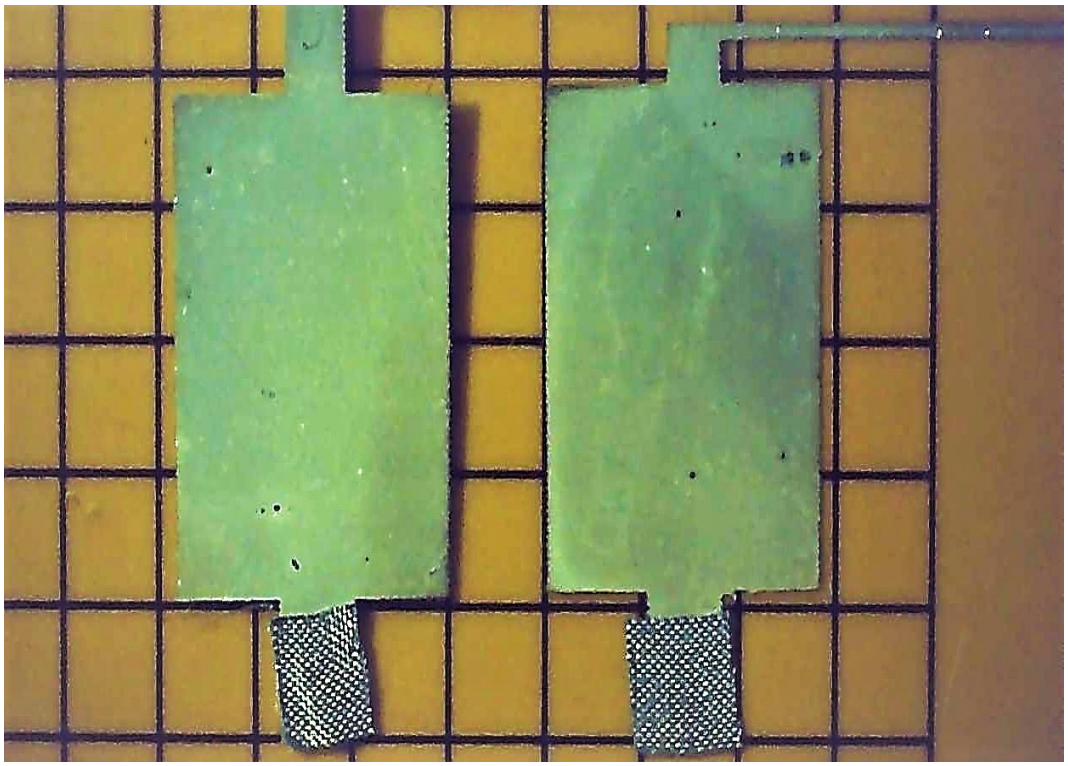

Figure 4.14: Pair of printed electrodes for BIA. On the pad, there is conductive tape for conductivity testing purposes.

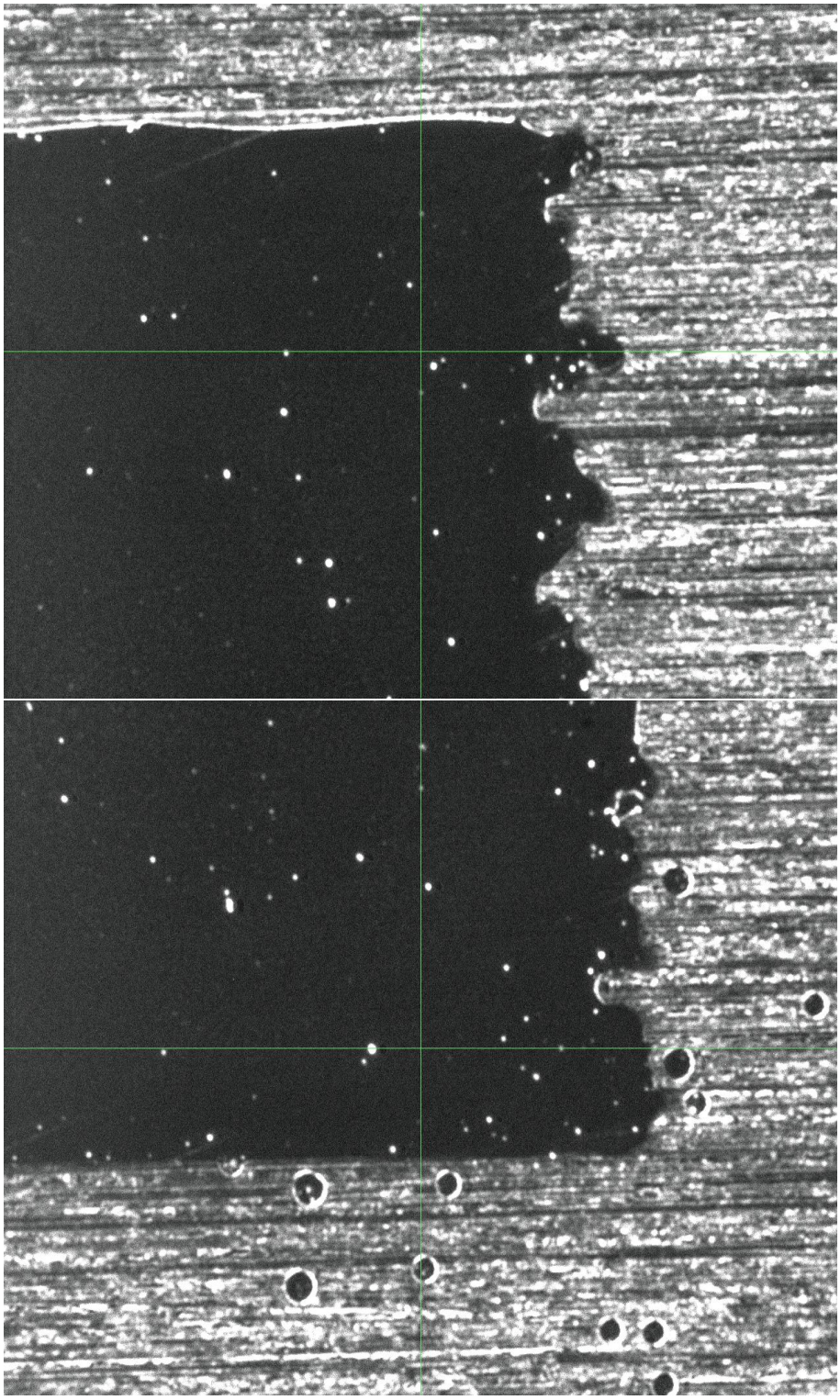

Figure 4.15: Angles of Bia electrodes

Chapter 5

IN VITRO CHARACTERIZATION

The present chapter will address *In Vitro* characterization performed to evaluate the performances of each of the printed sensors under controlled conditions. In order to improve the repeatability and the accuracy of the measurements, bench top certified instrumentation was exploited. For each sensor, at least a triplicate characterization was performed, trying to correlate changes in the quantifiable variables with simulated controlled changes in hydration conditions.

5.1 Temperature Sensors Characterization

The characterization of temperature sensors was done in order to test the changes in sensor resistance during an increase or decrease in the temperature of a body in contact with the sensor , opting for a range of temperature change between 33 and 42 °C. The range was chosen on the basis of the physiological temperature range , which in the case of a state of severe dehydration can reach around 42 °C.

The resistance R of the sensor was taken as a parameter for evaluating the functionality of the sensor. The set-up was created using a laboratory plate that is extremely sensitive to temperature variation , covered with a material layer with behaviors similar to artificial skin in terms of body resistance , where the sensor was placed on top , flanked by a thermometer for precise temperature measurement during the test period. Each test was performed by evaluating the functionality of 3 sensors at a time, evaluating the change in resistance during the temperature increase of the plate by 1 °C each step; then,a simple script on Matlab was created in order to calculate the values of the average of the sensors,the standard deviation, the R^2 index and Temperature Coefficient of Resistance(TCR). R-squared (R^2), or coefficient of determination, is a statistical measure that represents the proportion of the variance for a dependent variable that's explained by an independent variable or variables in a regression model.The formula of R^2 is

$$R^2 = 1 - \frac{\sum_{i=1}^{N}(y_i - \hat{y}_i)}{\sum_{i=1}^{N}(y_i - \overline{y}_i)} \tag{5.1}$$

where in numerator there is sum squared regression(the sum of the residuals squared) and the denominator there is the total sum of squares(the sum of the distance the data is away from the mean all squared). As it is a percentage it will take values between 0 and 1.

TCR is a very important and essential index to describe the behavior of a resistor as temperature changes. The characteristics of an RTD thermal sensor derive precisely from the value of its resistance, which changes depending on the temperature of the body to which the sensor rests. The changing resistance, defined as R, is calculated using the formula:

$$R = R_0(1 + \alpha\Delta T) \tag{5.2}$$

In the formula, R_0 is the value of resistance when the temperature is at 0 °C, T is the temperature change, and α is the Temperature coefficient of resistance,well known as TCR. The formula of TCR is:

$$TCR = \frac{(R2 - R1)}{(R1(T2 - T1))} \tag{5.3}$$

where T1 and T2 are the initial and final temperatures of the test respectively , R1 and R2 are the values of resistances associated with T1 and T2.

A initial test run was made on the first 3 sensors in order to evaluate the feasibility of the sensors, noting down what problems needed to be corrected within the measurements. After that,most accurate measurements were made in the next 6 sensors,and data of the optimized set up of the 6 sensors were reported.

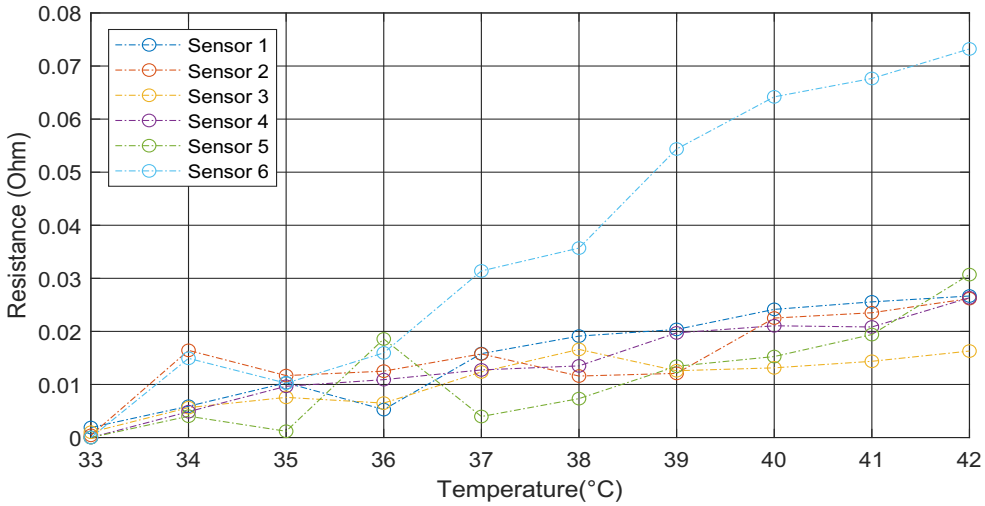

Figure 5.1: Chart of the 6 sensors

A bench top multimeter with a 6 digit resolution (Agilent E4980A Precision LCR

Meter) was selected to ensure the accuracy and the resolution required to monitor changes of resistances in the physiological range of temperature between 32 and 42 °C. The expected changes in resistance for this temperature range are in the order of 0.1 °C. Thus, a measurement tool with at least a 0.01°C accuracy is required, to avoid having instrumentation uncertainty higher than the resistance variation expected. Six different sensors were tested, exploiting the same setup. In detail, a layer of artificial skin was attached on top of a hot plate enabling manual control of surface temperature. The sensors were then attached with the sensing silver pattern in contact with the layer of artificial skin, together with an electronic thermometer to provide a feedback on the real temperature to be associated at each calibration step. The resistance of the sensors were measured when the temperature reached a steady state condition, every 1 °C increase, from 32 to 42 °C.

As it can be observed from Fig.5.1, all the sensors showed a linear dependency of resistance respect to temperature. A part from sensor 6 that shows a significantly different slope, all the other sensors showed comparable slopes, with an average value of and a standard deviation of 0.0046 Ω.

Regarding the TCR, the main difference could be observed comparing sensor 6 with all the others, as highlighted from the data reported in table 5.1. This different behavior can be explained considering the quite different geometry due to process variability that influenced the serpentine. Excluding sensor 6, the average TCR value calculated is 0.0027 +- 0.00062 1/°C. This value appears in agreement with values obtained in similar research works The quite high variability observed can be mainly related to variability in setup assembly and to process variability characterizing fast prototyping sensor fabrication as highlighted in recent literature reviewing printed resistive sensors. In order to reduce RSD and better highlight common trends among the different sensors, Relative Resistive Variation instead of absolute resistance values should be considered. As shown in Fig an average sensitivity of $0.247 \pm 0.056\%/°C$ with an average RSD reduced to 22%. This sensitivity corresponds to a Temperature Coefficient of Resistance (TCR) of 0.0025, which appears in agreement with works reporting printed temperature sensor [49].

Total graphs of the last 6 sensors were checked to underline differences in the result(fig 5.1). Temperature Coefficient of Resistance values of all 6 measured sensors were reported in the table 5.1.

Starting from the raw data acquired, the average values corresponding to each temperature tested was calculated and these values were exploited to compute the calibration curve. The linear regression performed resulted in an angular coefficient of a=0.0025, with a R^2 value of 0.9667, indicating a high relationship between the independent and dependent components of the regression curve.

An additional test to evaluate the dynamic response of the sensor to changes in temperature was performed. The test was carried out at the innovation hub of

Sensor	TCR(ppm/°C)
$Sensor1$	0.002
$Sensor2$	0.002
$Sensor3$	0.001
$Sensor4$	0.002
$Sensor5$	0.003
$Sensor6$	0.008

Table 5.1: Temperature Coefficient of Resistance (TCR)

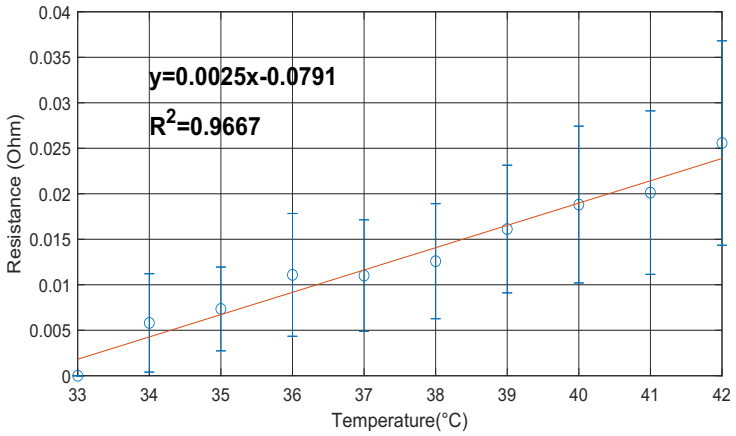

Figure 5.2: Sensor average values and standard deviation values

Microcity, EPFL University. A test through of a plate allowing manual temperature control was done, using synthetic skin-like patch layer to ensure more even heat distribution, varying the temperature from 33 °C to 42 °C, and reporting the temperature and resistance value every 10 seconds. A commercial thermometer was used for temperature measurement. Again, the resistance between the terminals of the serpentine RTD sensor was measured with a benchtop multimeter (digital multimeter 34401A, 6 $\frac{1}{2}$ -digit resolution, Keysigth Technologies, Santa Rosa, California (USA)), which greatly improved to the resolution of the results, as shown in the figure 5.3.

Fig.5.3 shows an example of the response, proving a good linearity ($R^2 = 0.99$) and a sensitivity of 0.044 Ω/°C, and suggesting that the sensor is suitable to record changes of temperature with a response time lower than 10 s, compatible with the usually slower variation time in vivo.

Sensor	TCR
$Sensor1$	0.00207831993922461

Table 5.2: Temperature Coefficient of Resistance (TCR) of single sensor(EPFL)

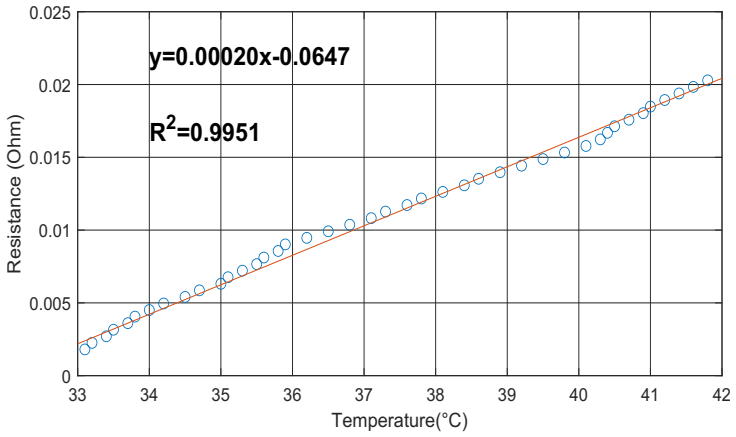

Figure 5.3: Sensor measurement at EPFL,Microcity

5.2 Interdigitated Sensors Characterization

Sensors for skin hydration monitoring were characterized simulating different skin hydration conditions attaching on top of the sensing area a layer of synthetic skin-like patch injected with controlled volumes of water, to obtain *In Vitro* hydration in the range between $0,0250 m\mathrm{L}/cm^2$ and $0.250 m\mathrm{L}/cm^2$. Real (Z_{real}) and imaginary part (Z_{imag}) of the impedance was measured in a range of frequencies between 100 Hz and 100 kHz. The same measurement was repeated for six sensors using a bench top Impedance analizer (Agilent E4990A, Precision LCR Meter). The frequency range was chosen based on the most suitable frequencies to be able to analyze the part just below the outer layer of skin. Hydration was administered in amounts of 0.0250 mL exactly below the intedigitated sensor, where there is a sensing area of 1 cm^2.

The results of the three sensors were highly promising. In the first sensor, as shown in Figure 5.4a, a clear distinction of the impedance values for each step was observed. In particular, both the real and imaginary parts of the impedance displayed good discrimination ability. The differences in impedance were more marked in the early steps, while in the final steps, the sensor reached a state of saturation, where the recorded impedance differences were significantly smaller but still clearly visible. The real part, which primarily describes the resistive behavior of the sensor, decreased with each step. This is because as the local humidity above the sensor increased, the sensor's conductivity improved due to the greater presence of electrolyte on the sensor's surface, resulting in a decrease in its resistive behavior. The imaginary part also decreased in modulus, making this value an excellent indicator of the local hydration state. It is important to note that the analysis was conducted over a range of frequencies. Through this test, it was verified that there is no single frequency that can better discriminate changes in the sensor's impedance, which is a positive outcome. Therefore, for an analysis of local hydration, any of the frequencies tested can be easily used

In the second sensor, results were similar to those of the first sensor. As shown in Figure 5.4b, the modulus of the impedance (both real and imaginary) decreased as the local humidity increased. However, the second sensor exhibited a much larger difference in impedance (in the case of the real part) for each step. For example, the impedance decreased by an order of magnitude from 10^5 Ohm to 10^4 between the first and fifth measurements, while in the first sensor it decreased by about 3000 Ohm. These differences are likely due to the printing method of the sensor, but they are not crucial for the detection of the hydration state. Future research could explore methods of sensor printing that ensure identical repeatability of the test across different sensors.

The third sensor displayed similar characteristics to the other two sensors, thus confirming the validity of the measurements and the functionality of the interdigitated sensor. As with the other two sensors (Figure 5.4c), the impedance modulus decreased in each step, perfectly discriminating the different local hydration states.

In figure 5.5a we can see the average behavior of all three sensors. The hydration value was converted to $\mu\mathrm{L}/cm^2$ knowing that the sensing area of the sensor is $1cm^2$. Additionally, both calibration curves built for Z_{real} and Z_{imag} measured at 100 Hz (fig.5.5b) showed the highest sensitivity ($-0.044\,k\Omega/(\mu\mathrm{L}/cm^2)$ for Z_{real} and $0.03\,k\Omega/(\mu\mathrm{L}/cm^2)$ for Z_{imag}) for volumes lower than $100\,\mu$L and a saturation after $200\,\mu$L, with sensitivities decreased to $-0.01\,k\Omega/(\mu\mathrm{L}/cm^2)$ for Z_{real} and to $-0.001\,k\Omega/(\mu\mathrm{L}/cm^2)$ for Z_{imag}. Good linearity could be observed both for the lower hydration fittings ($R^2 = 0.96$ for Z_{real} and $R^2 = 0.93$ for Z_{imag}) and for the higher hydration fittings ($R^2 = 0.98$ for Z_{real} and $R^2 = 0.89$ for Z_{imag}). Average linearity error of 2.5 % and 3 % of full-scale range could be computed respectively for real and imaginary part. Maximum values of linearity error were respectively of 6.5 % and 13.5 % for real and imaginary part. Regarding variability of the measurements, values of RSD lower than 35 % could be observed for both Z_{real} and Z_{imag}, with the highest values observed for lower volumes.

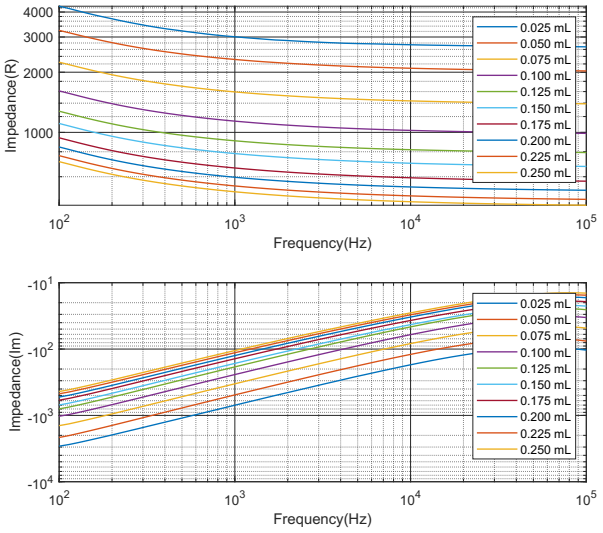

(a) Sensor 1 measurement

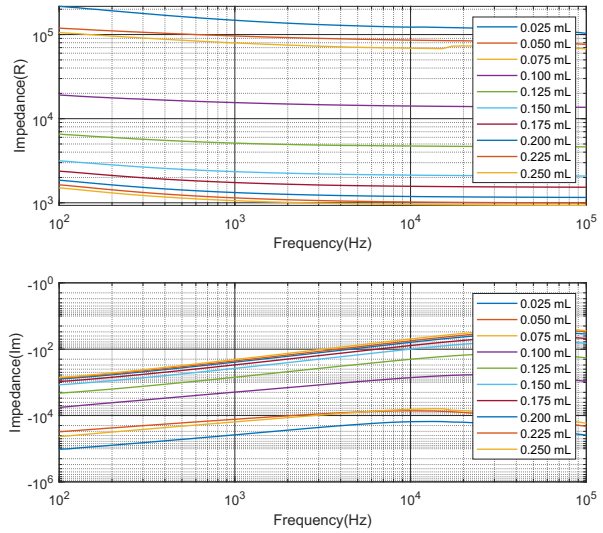

(b) Sensor 2 measurement

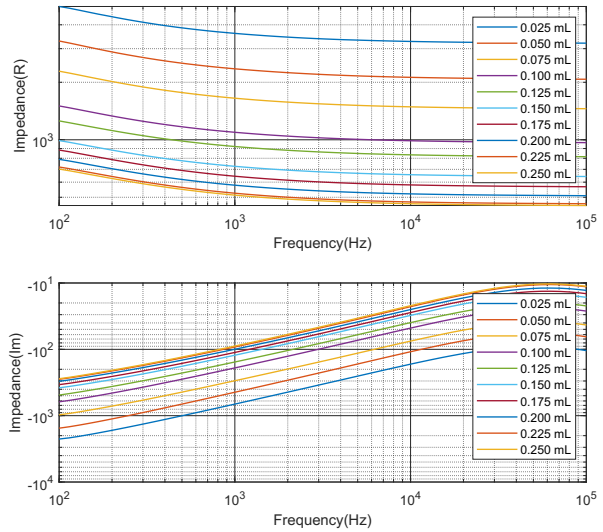

(c) Sensor 3 measurement

Figure 5.4: Measurements of all interdigitated sensors

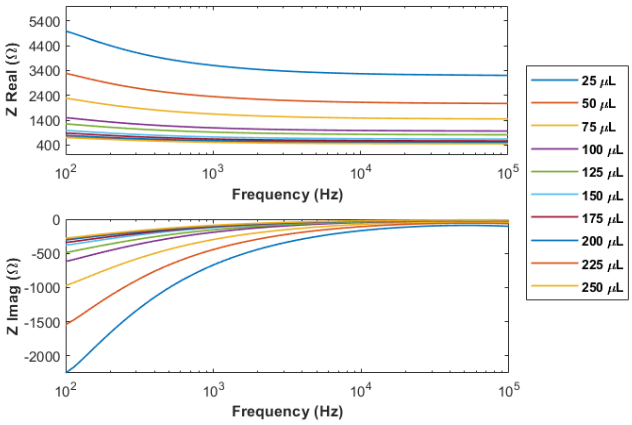

(a) Average behavior of interdigitate sensors

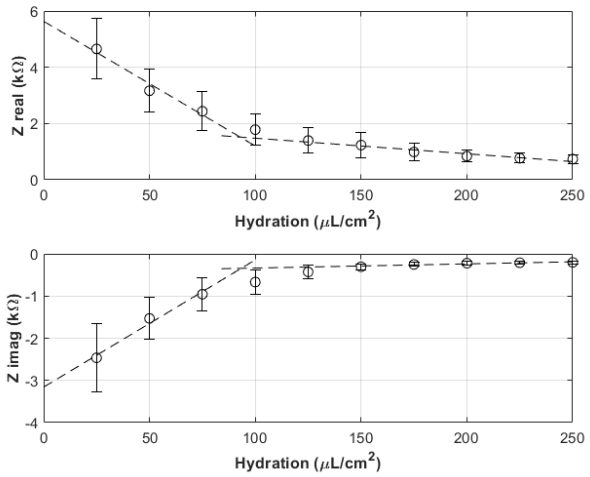

(b) Interdigitate sensors calibration

Figure 5.5: (a) Average behavior and (b) Calibration curve of interdigitated sensors

5.3 BIA Sensors Characterization

Characterization of the electrodes for Bioelectrical Impedance Analysis (BIA) was conducted to evaluate their functionality as the water content within the set-up increased. As shown in Figure 5.6, the set-up consisted of four BIA electrodes molded onto a plastic sheet, simulating the shape of the final device. The electrodes were attached to a layer of synthetic skin-like patch, which mimicked the resistance of the skin, and a layer of absorbent spongy matrix was added to simulate the contents of the arm. The set-up was held together by a plastic material that simulated the characteristics of bone. The entire set-up was connected to a Keysight E4980AL precision LCR meter, an impedance meter with a frequency range of 20 Hz to 20 MHz. The functionality of the instrument was evaluated by recording sensor impedance data as the water content of the absorbent tissue and spongy matrix increased. Impedance measurement was chosen as it provides an accurate measurement and enables the identification of a specific frequency that can optimally discriminate changes in water content. After numerous trials to optimize the set-up, a test protocol was established in which each measurement step was performed by adding 1 mL of water until 10 mL was injected into the tissue. In each step, three measurements were taken and the average of the three values was calculated to obtain a more accurate measurement. In addition, the liquid-free state (dry state) was also measured to ensure that the initial measurements were correct. Each measurement was made with an alternating current of 10 mV, in a frequency range of 100 Hz to 200 kHz, using 61 logarithmically spaced recording points, similar to what was observed in the *In Vitro* experiment for interdigitated sensors.

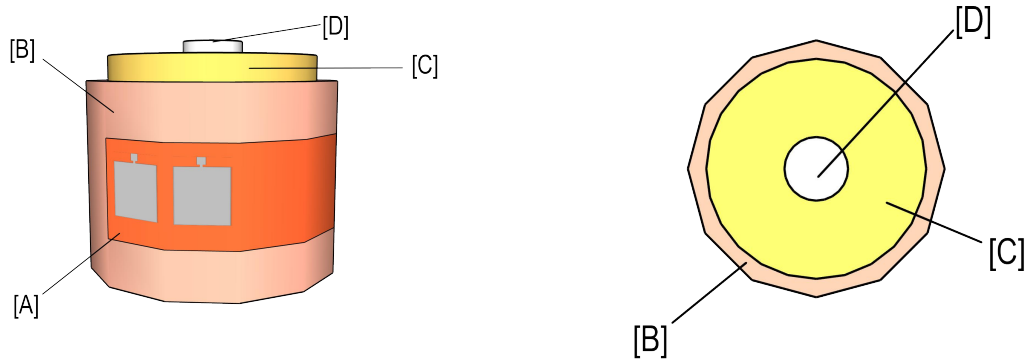

Figure 5.6: Set up for BIA electrodes *In Vitro* tests,[A] is the plastic material with the silver electrodes,[B] is the absorbent material layer, [C] is the sponge matrix layer and [D] is the plastic-bone material.

Test measurements were initially conducted on two prototype sensors to experiment with the set-up and ensure the functionality of the sensors. Subsequently, tests were performed on three sensors that exhibited correct measurement and printing characteristics, and the results are presented in the figures.

In Figure 5.7a, we can see in the upper portion, values of the real impedance in a range between 100 Hz and 10 kHz, while in the lower portion, values of the imaginary impedance in the same frequency range. These measurements were highly effective: as the water content within the set-up increases, a decrease in the modulus of the impedance (both real and imaginary) is observed, similar to the behavior of interdigitated sensors.

Particular attention should be paid to the frequencies: it is clear that for specific values, there is a clear discrimination of the impedance value. This means that in order to accurately assess the internal hydration state through BIA, it is necessary to select precise frequency ranges, so that the acquired impedance values are distinguishable. In this case, for sensor 1, a frequency range between 100 Hz and 30 kHz for the real part, and a range between 100 Hz and 100 kHz for the imaginary part, are frequencies that allow precise analysis of the impedance value (and thus, of the hydration state). Higher values, such as frequencies above 1000 Hz for the real part, resulted in a drastic decrease in the impedance differences, until a condition of overlapping between the reading values was reached.

Subsequent tests on sensors 2 and 3 were highly satisfactory and comparable to the measurements made in the first test, confirming the validity of the measurements and the functionality of the sensors. The characterization exhibited differences in terms of the size of the impedance values, which should be normalized, but the graphs clearly demonstrate that the behavior of the sensors is the same during the tests.

In Figure 5.7b, we observe a decrease in the modulus of the impedance values. By focusing on the frequency values that best characterize the hydration state, we can identify a range of 100-20000 Hz for real impedance and a range of approximately 100-50000 Hz for imaginary impedance. Notably, above 2 mL, the differences in impedance between each step become relatively small, yet still readily measurable by the impedance meter.

In Figure 5.7c, it was also observed a decrease in the modulus of the impedance values. Similar to the previous figure, by focusing on the frequency values, it can be distinguished a range of 100-20000 Hz for real impedance and a range of approximately 100-50000 Hz for imaginary impedance. This allows for greater discrimination of the measured impedance values. It is worth noting that, particularly in the real impedance section, values above the indicated range show measurements that do not correlate with increasing hydration states, making it difficult, if not impossible, to interpret the results. The results of the experiments were successful in demonstrating the functionality and applicability of the BIA sensors. Additionally, a range of frequencies were established where a difference in hydration could be accurately discriminated. Furthermore, it can be noted that the imaginary impedance values have a wider range of frequencies where different hydration states can be

distinguished compared to the real impedance values.

The graphs 5.8a and 5.8b show the average values of sensor measurements and the calibration curve of the sensors, respectively. The hydration value was converted to $\mu L/cm^2$ knowing that the sensing area of the sensor is $1cm^3$

Both Z_{real} and Z_{imag} showed the highest sensitivity toward hydration levels lower than $60\,\mu L/cm^3$ (sensitivity of $-0.37\,k\Omega/(\mu L/cm^3)$ for Z_{real} and of $0.44\,k\Omega/(\mu L/cm^3)$ for Z_{imag}). For levels of hydration higher than $80\,\mu L/cm^3$ the system showed lower sensitivities ($-0.04\,k\Omega/(\mu L/cm^3)$ for Z_{real} and $0.01\,k\Omega/(\mu L/cm^3)$ for Z_{imag}). Good linearity could be observed in two ranges: for lower hydration from 2 to $60\,\mu L/cm^3$ ($R^2 = 0.97$ for Z_{real} and $R^2 = 0.93$ for Z_{imag}) and for higher hydration from 80 to $200\,\mu L/cm^3$ ($R^2 = 0.91$ for Z_{real} and $R^2 = 0.83$ for Z_{imag}). Average linearity error of 2.7 % and 3.7 % of full-scale range could be computed respectively for real and imaginary part of the impedance of interdigitated sensors. Maximum values of linearity error were respectively of 11.5 % and 10 % for real and imaginary part. Regarding sensors variability a quite high RSD could be observed mainly due to operator-dependent calibration process exploited. However, RSD lower than 30 % for Z_{real} appear in agreement with RSD showed by similar BIA analyzers [53].

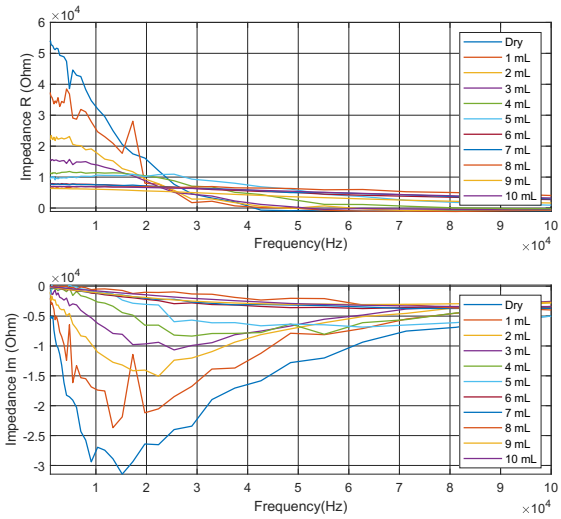

(a) Sensor 1 measurement

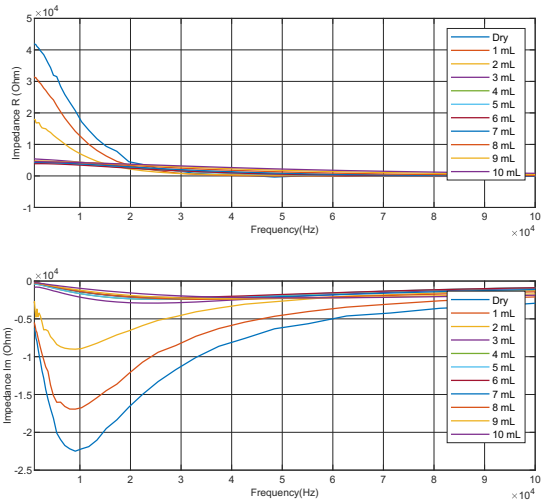

(b) Sensor 2 measurement

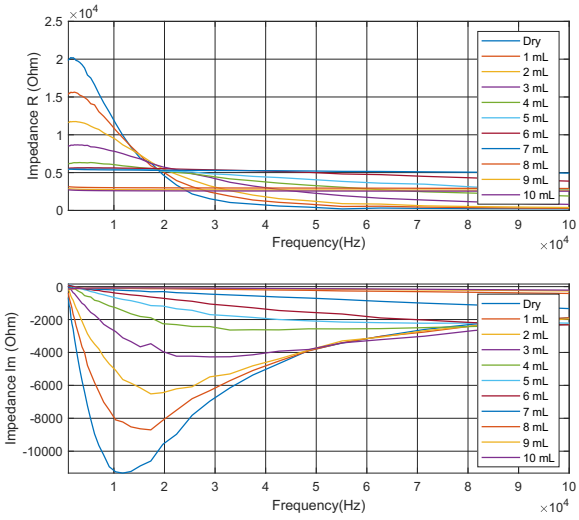

(c) Sensor 3 measurement

Figure 5.7: Measurements of all BIA electrodes

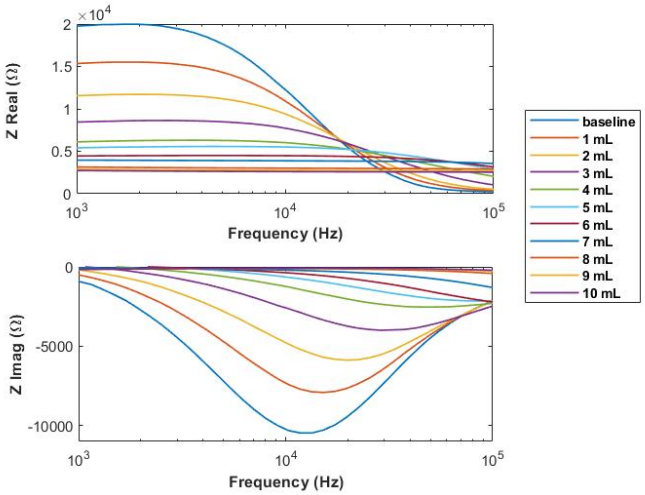

(a) Average behavior Bio-impedance electrodes measurements

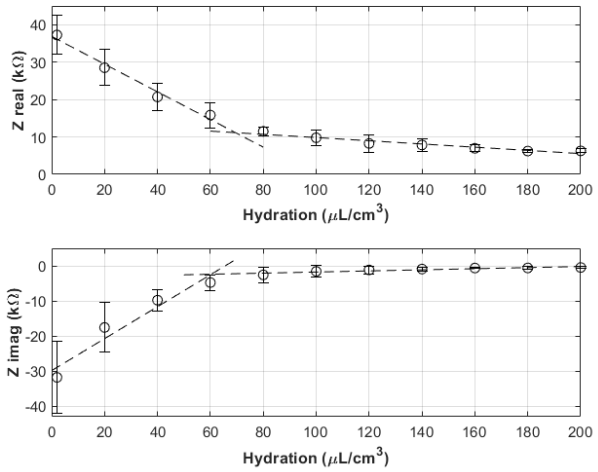

(b) Calibration curve BIA electrodes

Figure 5.8: (a) Average behavior and (b) Calibration curve of BIA electrodes

Chapter 6

IN VIVO EXPERIMENTS

In Vivo experiments addressed two specific aims. A first set of measurements was performed to evaluate the variability among different printed sensors used on the same site of the same subject at the same time point. A second set of tests was instead performed to provide a validation of the use of those sensors for monitoring different hydration conditions in two different healthy volunteers.

6.1 *In Vivo* characterization

In Vivo characterization was performed by attaching each sensor under test on the skin of a volunteer in their wrist and secured with irritation-free adhesive medical tape.For all the sensors, one measurement at 10 kHz was performed for 10 minutes to test the sensors' reliability. Three temperature sensors, three interdigitated sensors, and two BIA electrode in the 4-wire configuration were used for the characterization.

In 6.1 it can be seen that all three sensors are subject to strong variability.The variability between the sensors is given by the differences during inkjet printing, while the variability during the measurement of the same sensor can be explained by the instability of the sensor's bearing surface, i.e., the skin, either by its geometry or its surface characteristics. Both initial and final sweep behavior is similar in all sensors. The percentage differences of the initial and final sweeps are very small: in the case of the first sensor, an increase of 0.3960% was obtained, while in the second and third sensors, a decrease in the percentage differences is obtained, -0.1717% and -0.0235% respectively.

First and second sensors shows an initial transitory phase of around 300s, after which a steady state is reached. This can be explained by considering the physical time required to reach the body's temperature from the initial room temperature. An average relative change in resistance of 3.1% was computed going from a temperature of 25°C to a body temperature of 36.8°C. This corresponds to a sensitivity of 0.262%/°C, which agrees with the value calculated *in vitro* (0.258%/°C)

The average response of interdigitated sensors (fig.6.2) for local hydration moni-

toring shows an initial transient phase of around 300s before reaching a steady state value. This suggests considering an initial conditioning period when the bracelet is worn, which is necessary to reach a stable state. The relaxation behavior is strongly evident in this type of sensor: analyzing the curve, the percentage difference between the initial and final sweeps of each curve measure -23.4055% for the first sensor, -31.4128% for the second and -52.8981% for the third, respectively.

Analysis of the data obtained from the interdigitated sensors revealed that the time required to reach 90% of the steady-state value for each sensor can be determined. The results showed that it took 276 s, 269 s, and 334 s, respectively, for the first, second, and third sensors to reach 90% of the steady-state value, with an average of 293 s (4.88 min) to reach this threshold. These values were found to be higher, on average, compared to those obtained from the BIA sensors, which required an average of 160.75 s (2.67 min) to reach 90% of the steady-state value, with individual times of 216 s and 105.5 s.

The average steady-state value observed is equal to $886 \pm 250\Omega$ and, depends on the calibration performed in vitro, corresponds to a water content of $200\,\mu\mathrm{L}/cm^3$. Considering the thickness of around 3 mm of the artificial skin layer, this value corresponds to a three-dimensional value of $660\,\mu\mathrm{L}/cm^3$ or, if expressed in percentage to 66% of water content. This appears in agreement with the typical physiological dermal water content [55].

Impedance graphs of the two sets of electrodes were plotted in 6.3, and the sweep was represented in the form of a Cole plot, to better highlight the behavior of the electrodes as the frequency changes.As can be seen from the Cole's graph and the behavior of the impedances, the electrode groups exhibit the same behavior. In particular, the impedance relaxation phase after the 10-minute test is also very noticeable here, with an approximate value of 142.5 Ω for the first electrode group and 101.1 Ω in the second electrode group.

The average steady-state response measured after this transitory is $78.6 \pm 20\Omega$. Considering the linear calibration that can be obtained from *In Vitro* tests and extending it beyond the range evaluated in the *In Vitro* setup, the impedance value measured corresponds to a hydration value of $554\,\mu\mathrm{L}/cm^3$ or if expressed in percentage to 55.4% of water content. This value appears in agreement with total body water comprises approximately 50 to 60% of adult body weight with a range from 45 to 75%. For the range between 20 to 29 years, corresponding to one of the volunteers tested with printed sensors, the literature reports an average body water percentage of 56% [54]. These results strongly confirm the ability of printed BIA electrodes to measure body water content.

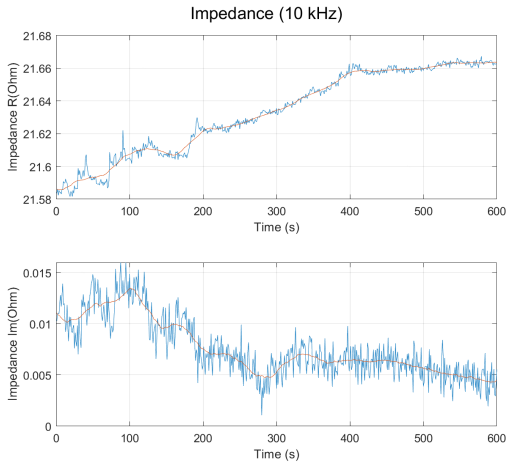

(a) Impedance sensor 1

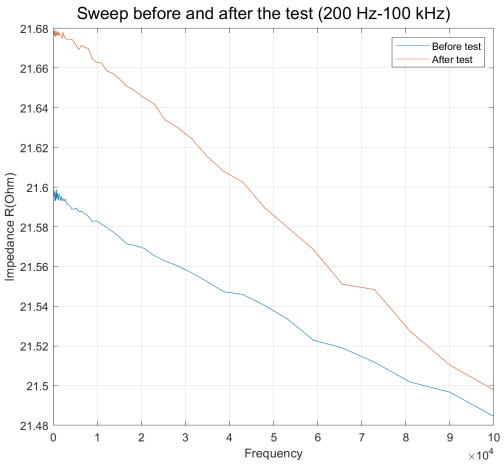

(d) Sweep sensor 1

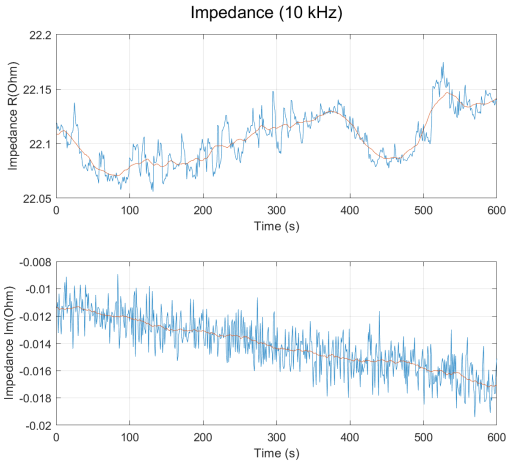

(b) Impedance sensor 2

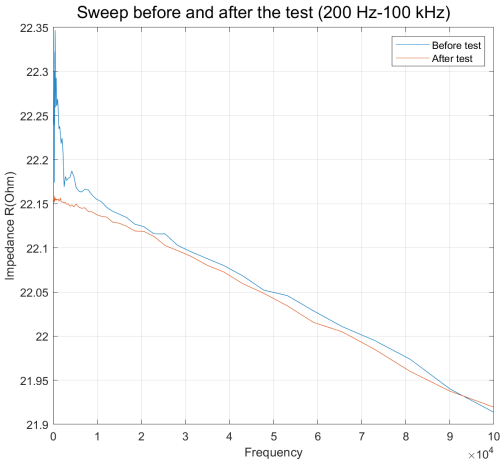

(e) Sweep sensor 2

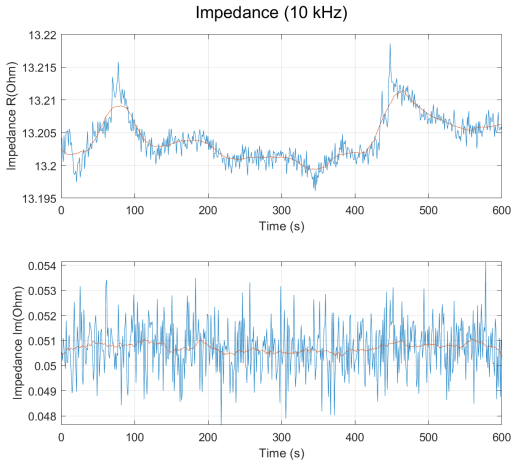

(c) Impedance sensor 3

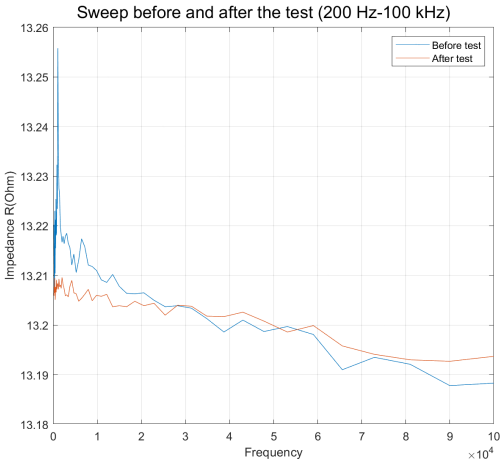

(f) Sweep sensor 3

Figure 6.1: Temperature sensors characterization

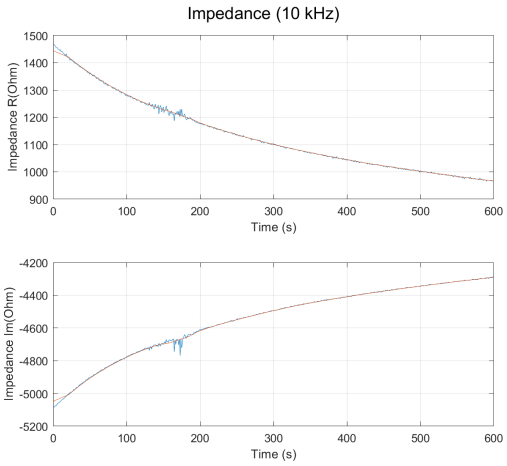

(a) Impedance sensor 1

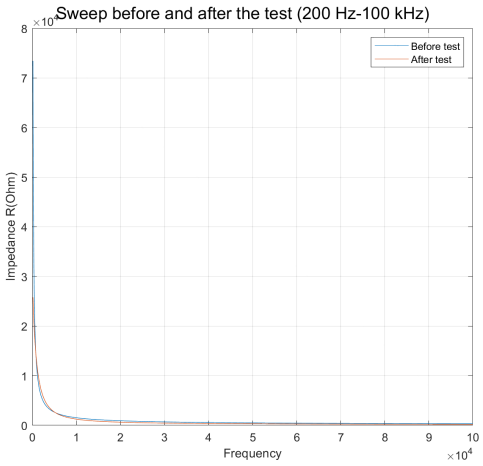

(d) Sweep sensor 1

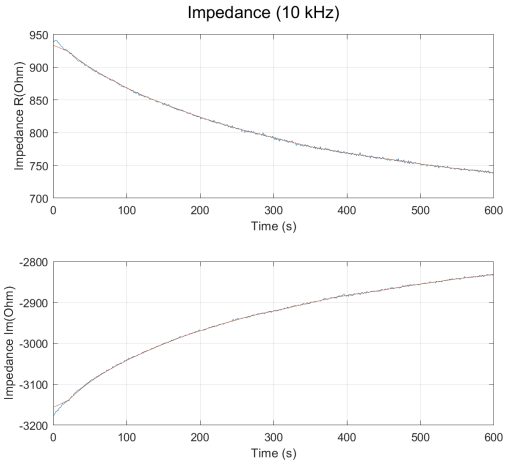

(b) Impedance sensor 2

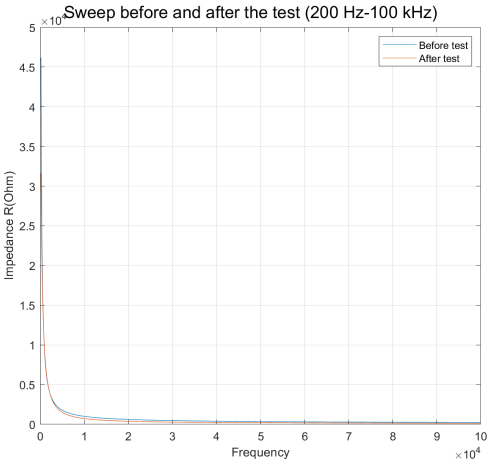

(e) Sweep sensor 2

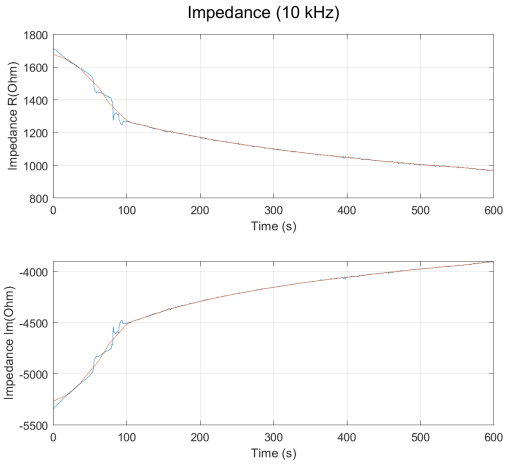

(c) Impedance sensor 3

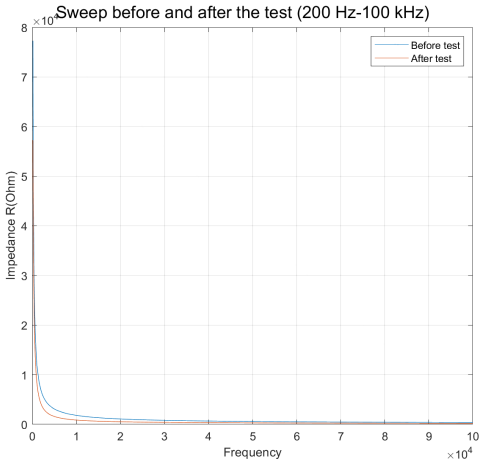

(f) Sweep sensor 3

Figure 6.2: Interdigitate sensors characterization

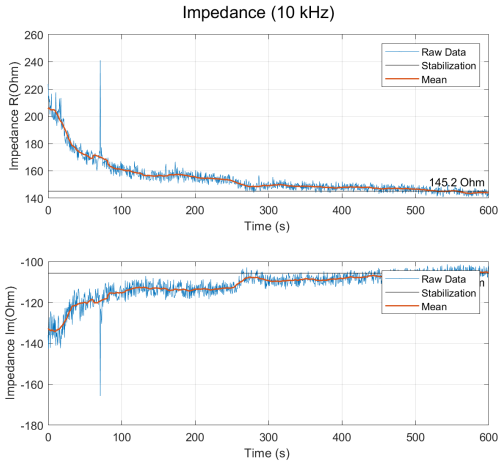

(a) Impedance sensor 1

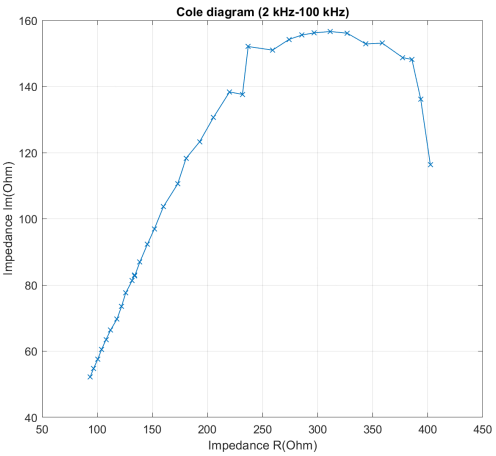

(c) Cole sensor 1

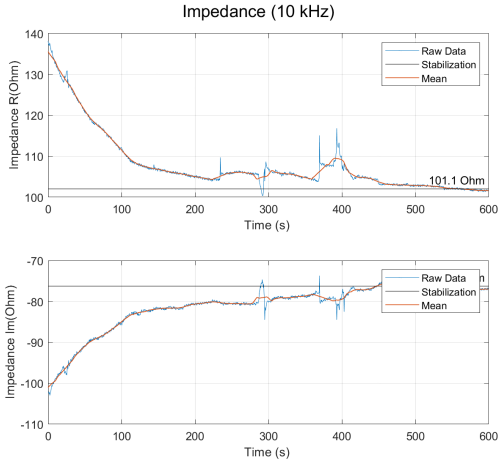

(b) Impedance sensor 2

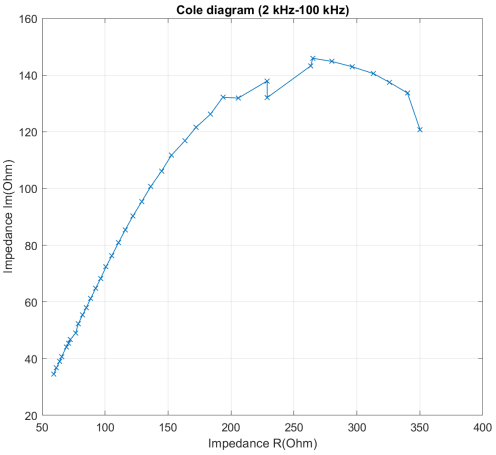

(d) Cole sensor 2

Figure 6.3: BIA sensors characterization

6.2 *In Vivo* validation for hydration monitoring

This chapter addresses the results obtained from *In Vivo* validation of the printed bracelet interfaced with portable customized electronics. The goal was to optimize the device's size by reducing the sensors, resulting in a more compact cuff that is compatible with a wide range of individuals. The data collected included body temperature, hours from water intake at the time of measurement, and impedance measurements from the temperature sensor, interdigitated sensor, and BIA electrodes. Data were recorded from two healthy subjects under resting conditions. The temperature was not included since it is a parameter that presents significant changes only in case of moderate dehydration, while these measurements were performed on healthy volunteers in a relatively short time window after water intake. Therefore, only small variations are expected.

For both subjects, local and whole body impedance was measured at different time points (t1 = 1h, t2 = 2h, t3 = 3h) after the water intake. The first measurement is performed after 1 hour to allow the body to absorb water. The measurements were performed on the wrist, acquiring the impedance at 10 kHz for 5 minutes.

It was employed a sweep analysis, also known as a Cole-Cole plot, to evaluate the changes in both real and imaginary impedance in a chosen frequency spectrum using BIA electrodes. The frequency range used was between 10kHz and 200kHz. In the figure 6.4, were selected sweeps that correlated with increasing hours from water intake. The selected sweeps are measurement 4-6(subject 1) and measurements 11-12-13(subject 2). From the graph, it can be observed that the differences in impedance measurements are clearly visible, where in the case of subject 1, the impedance values of measurement 6 (corresponding to 3 hours from water intake) are significantly higher than measurement 4 (corresponding to 1 hour from water intake). The same pattern can be seen in subject 2, where measurement 13(3 hours from water intake) is significantly higher than measurement 11(1 hour of fasting), but there are no major differences from measurement 12(2 hours from water intake).

In Figure 6.5a and 6.5b, the interdigitated and BIA sensor measurements of two subjects are displayed. The interdigitated sensor shows a noteworthy trend: the impedance value decreases during the second hour without water intake and then rises again in the third hour. This trend is most prominent in the first subject, while it is less pronounced in the second subject because the first two measurements were not taken during the steady-state phase. The hypothesis for this behavior is that the local water change occurs approximately 2 hours after the last water intake, causing a drop in local impedance. In the case of the BIA electrodes, the results presented in the graph demonstrate the expected behavior. As the elapsed time since the last water intake increases, a corresponding increase in impedance (real) is observed, consistent with the expectations set forth in prior documentation and

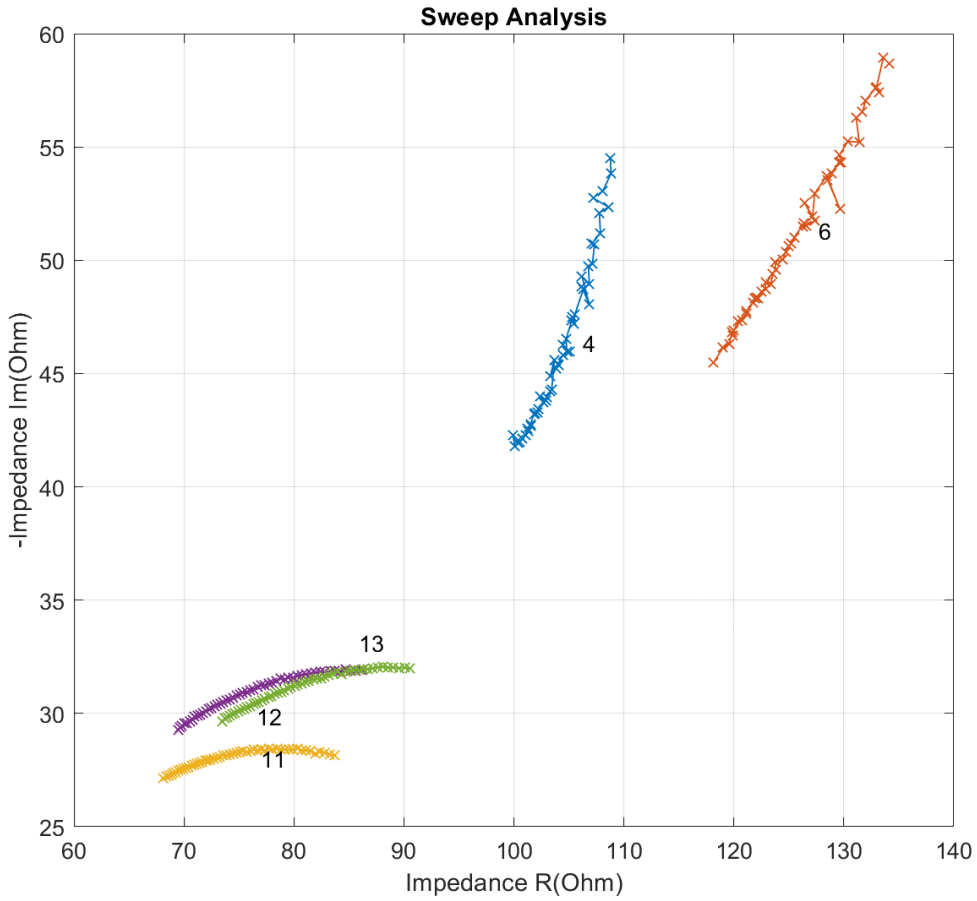

Figure 6.4: Sweep Analysis.

validated through *In Vitro* testing.

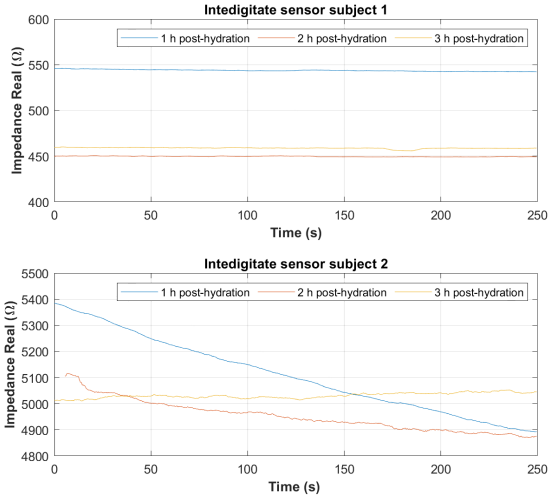

(a) Last 30 seconds of interdigitate sensor measurements of both groups.

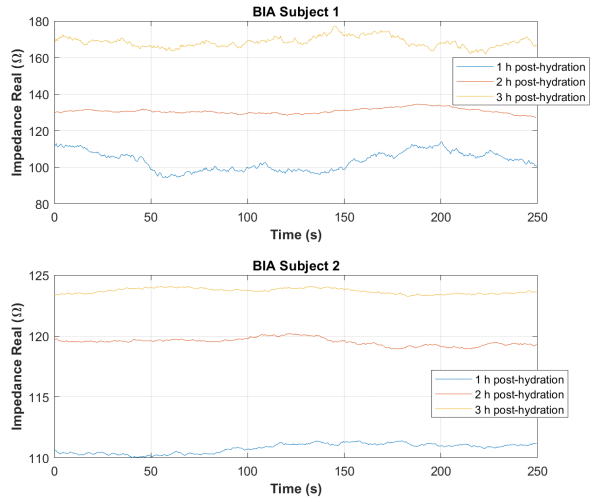

(b) Last 30 seconds of BIA sensor measurements of both groups.

Figure 6.5: Impedance/Time graph of interdigitated sensors and BIA electrodes.

Figures 6.6a and 6.6b present the average measurements of the impedance values of the interdigitated sensor and BIA electrodes. Consistent with what has been said about the behavior of the interdigitates, the graph seems to assume a delay in local hydration during the second hour without water intake, and then resumes with an increase in impedance during the third hour. The same trend is observed in both subjects. In both subjects BIA electrodes show a clear upward trend as the time without water intake increases. The visible difference is that the impedance increase is greater in subject 1 than in subject 2.

To clarify the disparities between the two subjects' measurements, normalizations were applied. The normalization procedure for the interdigitated electrodes involved subtracting the initial value and applying FSR normalization, as depicted

in Figure 6.7a. This highlights the percentage change from the initial value for each subject and highlights the decrease in impedance observed in the second hour (due to delayed local hydration), followed by an increase in the third hour. Although inter-subject variability is evident, it is attributed to the unique characteristics of each subject.

For the BIA sensors, a normalization procedure involving subtraction of the minimum value was performed and is presented in Figure 6.7b. This normalization is crucial in revealing the similarities in the behaviors of the BIA electrodes between the two subjects, with a difference of approximately 20% FSR in the measurement taken after 2 hours.

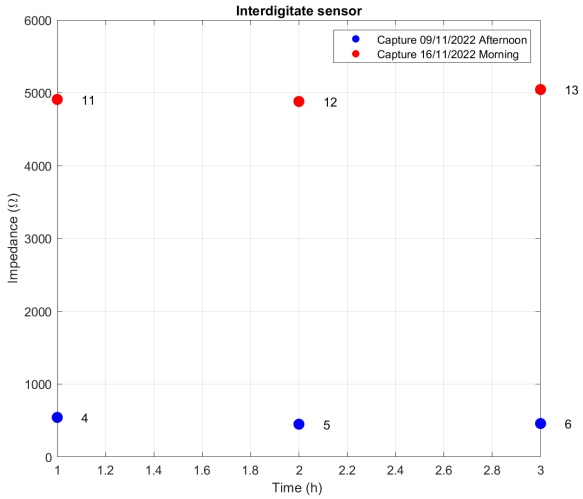

(a) Interdigitate sensor measurements 4,5,6,11,12,13. The correlation is between 4-5-6 and between 11-12-13.

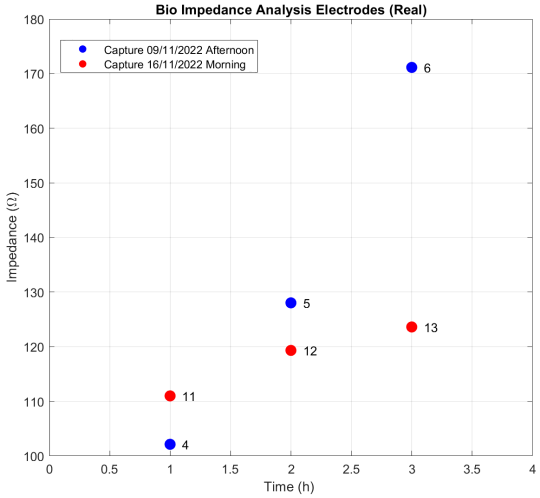

(b) BIA electrodes impedance(Real) of measurements 4,5,6,11,13. The correlation is between 4-5-6 and between 11-13

Figure 6.6: Impedance/Hours from water intake graph of interdigitated sensors and BIA electrodes.

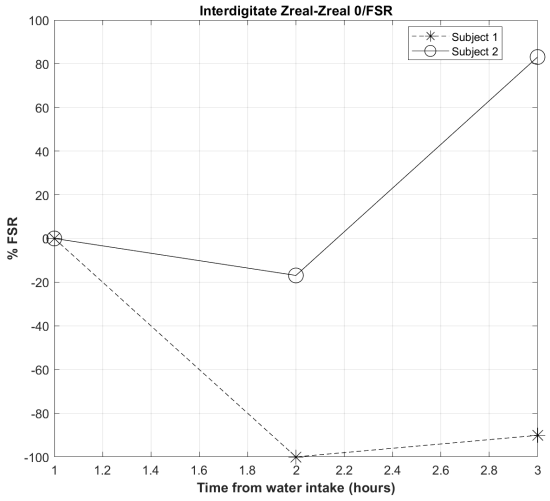

(a) Interdigitate FSR normalization by subtracting the initial value.

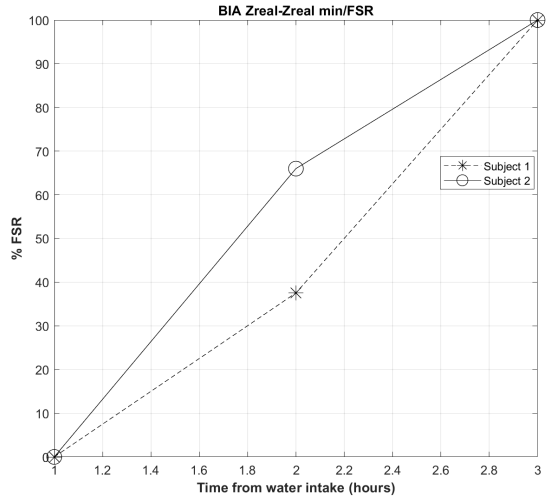

(b) BIA FSR normalization by subtracting the minimum value.

Chapter 7

CONCLUSION AND FUTURE DEVELOPMENTS

In conclusion, this work demonstrates the preliminary *In Vivo* testing of a multi-sensory dehydration monitoring platform, combining the low-cost, flexible bracelet with customized, light-weighting, portable electronics. The device utilizes a combination of resistance,local hydration monitoring, and body global composition analysis to provide an accurate and non-invasive measurement of hydration levels. The results of the study indicate that the prototype is able to measure hydration levels and detect changes in hydration status. In particular, sensors *In Vitro* characterization allowed to confirm the ability of the sensing element to follow changes in the targeted quantities and enables the selection of a single frequency for simplifying measurements with the portable electronics. *In Vivo* characterization showed results in agreement with the measurements performed in Vitro, after an initial time needed to reach the steady state. Preliminary *In Vivo* tests performed on two subjects confirmed the possibility of detecting proportional changes in both local and global impedance due to changes in the body's hydration status.

Future developments for the device will mainly focus on improving the design of sensors and interconnection with portable electronics, testing in particular, reproducibility and stability of measurements. Also, the device could incorporating additional sensors to measure other important hydration-related parameters such as blood glucose levels or electrolyte levels. Another possible development is the detection of arterial pulsation for capturing ECG data using electrodes for bioimpedance analysis. Other possible avenue for future development would be to optimize the device's design to make it more compact and user-friendly. It could also be useful to conduct further studies to validate the device's performance in different population groups and under different environmental conditions. Additionally, it could be interesting to investigate the possibility of integrating the device with a mobile application that would allow users to track their hydration levels over time, providing real-time feedback and personalized hydration recommendations. With develop-

ments in the field, the possibility of implementing AI to classify the subject's state and suggest water replenishment could be an advantageous direction for the tool, but large data collections are needed to implement it successfully.

Bibliography

[1] *Popkin BM, D'Anci KE, Rosenberg IH. Water, hydration, and health. Nutr Rev. 2010 Aug;68(8):439-58. doi: 10.1111/j.1753-4887.2010.00304.x. PMID: 20646222; PMCID: PMC2908954.*

[2] *Tobias A, Ballard BD, Mohiuddin SS. Physiology, Water Balance. [Updated 2022 Oct 3]. In: StatPearls [Internet]. Treasure Island (FL): StatPearls Publishing; 2022 Jan-.*

[3] *P. Kassanos, F. Seichepine, and G.-Z. Yang, "A comparison of front-end amplifiers for tetrapolar bioimpedance measurements," IEEE Transac tions on Instrumentation and Measurement, vol. 70, 2021. Cited by: 2; All Open Access, Hybrid Gold Open Access.*

[4] *D. Barmpakos and G. Kaltsas, "A review on humidity, temperature and strain printed sensors—current trends and future perspectives," Sensors, vol. 21, no. 3, 2021.*

[5] *IoT technologies for Active Ageing: an Overview of the Elderly Dehydration Case Alessandra Galli,Giada Giorgi,Claudio Narduzzi,Giacomo Peruzzi,Alessandro Pozzebon and Sarah Tonello, Department of Information Engineering, University of Padova, Italy*

[6] *Kyle UG, Bosaeus I, De Lorenzo AD, Deurenberg P, Elia M, Gómez JM, Heitmann BL, Kent-Smith L, Melchior JC, Pirlich M, Scharfetter H, Schols AM, Pichard C (October 2004). "Bioelectrical impedance analysis–part I: review of principles and methods". Clinical Nutrition. 23 (5): 1226–1243. doi:10.1016/j.clnu.2004.06.004*

[7] *Foster, K R; Lukaski, H C (September 1996). "Whole-body impedance–what does it measure?". The American Journal of Clinical Nutrition. 64 (3): 388S–396S.*

[8] *T. Huynh, R. Jafari, and W.-Y. Chung, "A robust bioimpedance structure for smartwatch-based blood pressure monitoring," Sensors (Switzerland), vol. 18, no. 7, 2018*

[9] *W. Ji, J. Zhu, W. Wu, N. Wang, J. Wang, J. Wu, Q. Wu, X. Wang, C. Yu, G. Wei, L. Li, and F. Huo, "Wearable sweat biosensors refresh personalized health/medical diagnostics," Research (Washington, D.C.), vol. 2021, p. 9757126, 10 2021.*

[10] *Kyle U.G., Bosaeus I., De Lorenzo A.D., Deurenberg P., Elia M., Gómez J.M., Heitmann B.L., Kent-Smith L., Melchior J.-C., Pirlich M. Bioelectrical impedance analysis—Part i: Review of principles and methods. Clin. Nutr. 2004;23:1226–1243*

[11] *Martinsen O.G., Grimnes S. Bioimpedance and Bioelectricity Basics. Academic Press; Waltham, MA, USA: 2011.*

[12] *De Lorenzo A., Andreoli A., Matthie J., Withers P. Predicting body cell mass with bioimpedance by using theoretical methods: A technological review. J. Appl. Physiol. 1997;82:1542–1558.*

[13] *Olde R.M., Deurenberg P., Jansen R., Van't Hof M., Hoefnagels W. Validation of multi-frequency bioelectrical impedance analysis in detecting changes in fluid balance of geriatric patients. J. Am. Geriatr. Soc. 1997;45:1345–1351*

[14] *Yao S, Myers A, Malhotra A, Lin F, Bozkurt A, Muth JF, Zhu Y. A Wearable Hydration Sensor with Conformal Nanowire Electrodes. Adv Healthc Mater. 2017 Mar;6(6). doi: 10.1002/adhm.201601159. Epub 2017 Jan 27. PMID: 28128888.*

[15] *Agarwal, D.; Randall, P.; White, Z.; Bisnette, B.; Dickson, J.; Allen, C.; Chamani, F.; Prakash, P.; Ade, C.; Natarajan, B. A Non-Invasive Hydration Monitoring Technique Using Microwave Transmission and Data-Driven Approaches. Sensors 2022, 22, 2536. https://doi.org/10.3390/s22072536*

[16] *S. Diaham, "Polyimide in electronics: Applications and processability overview," in Polyimide for Electronic and Electrical Engineering Applications (S. Diaham, ed.), ch. 1, Rijeka: IntechOpen, 2021*

[17] *D. Barmpakos and G. Kaltsas, "A review on humidity, temperature and strain printed sensors—current trends and future perspectives," Sensors, vol. 21, no. 3, 2021.*

[18] *Liew, Q.J.; Aziz, A.S.A.; Lee, H.W.; Lee, M.W.; Hawari, H.F.; Md Khir, M.H. Inkjet-Printed Flexible Temperature Sensor Based on Silver Nanoparticles Ink. Eng. Proc. 2020, 2, 3. https://doi.org/10.3390/ecsa-7-08216*

[19] *Ramsay, DJ. Homeostatic control of water balance. In: Arnaud, MJ., editor. Hydration Throughout Life. Montrouge: John Libbey Eurotext; 1998. p. 9-18.*

[20] *Davies I, O'Neill PA, McLean KA, Catania J, Bennett D. Age-associated alterations in thirst and arginine vasopressin in response to a water or sodium load. Age Ageing. 1995; 24:151–159. [PubMed: 7793338]*

[21] *Cheuvront SN, Carter R 3rd, Sawka MN. Fluid balance and endurance exercise performance. Curr Sports Med Rep. 2003; 2:202–208. [PubMed: 12834575]*

[22] *Cian C, Barraud PA, Melin B, Raphel C. Effects of fluid ingestion on cognitive function after heat stress or exercise-induced dehydration. Int J Psychophysiol. 2001; 42:243–251. [PubMed: 11812391]*

[23] *Cian C, Koulmann PA, Barraud PA, Raphel C, Jimenez C, Melin B. Influence of variations of body hydration on cognitive performance. J Psychophysiol. 2000; 14:29–36*

[24] *Schoen EJ. Minimum urine total solute concentration in response to water loading in normal men. J Appl Physiol. 1957; 10:267–270. [PubMed: 13428657]*

[25] *Callegaro, C., Moraes, R., Negrão, C. et al. Acute water ingestion increases arterial blood pressure in hypertensive and normotensive subjects. J Hum Hypertens 21, 564–570 (2007). https://doi.org/10.1038/sj.jhh.1002188*

[26] *Bak A, Tsiami A, Greene C. Methods of Assessment of Hydration Status and their Usefulness in Detecting Dehydration in the Elderly. Curr Res Nutr Food Sci 2017;5(2). doi : http://dx.doi.org/10.12944/CRNFSJ.5.2.01*

[27] *Guyton A. Textbook of medical physiology. 5th ed. Philadelphia: Saunders; (1976).*

[28] *Thomas DR, Cote TR, Lawhorne L, Levenson SA, Rubenstein LZ, Smith DA, et al. Understanding clinical dehydration and its treatment. J Am Med Dir Assoc; vol.9(5), pp.292-301 (2008 Jun)*

[29] *Longmore JM. Oxford handbook of clinical medicine. Oxford: Oxford University Press; (2007*

[30] *Armstrong LE. Assessing hydration status: The elusive gold standard. J Am Coll Nutr; vol.26(5 Suppl): pp.575S-584S (2007 Oct)*

[31] *Armstrong LE. Hydration Assessment Techniques. Nutr Rev; vol.63(S1), pp.40-54 (2005)*

[32] *Manz, Friedrich and Andreas Wentz. "24-h hydration status: parameters, epidemiology and recommendations." European Journal of Clinical Nutrition 57 (2003): S10-S18.*

[33] *Jang, M.; Kim, H.-D.; Koo, H.-J.; So, J.-H. Textile-Based Wearable Sensor for Skin Hydration Monitoring. Sensors 2022, 22, 6985. https://doi.org/10.3390/s22186985*

[34] *Kurosumi, Kazumasa; Shibasaki, Susumu; Ito, Toshiho (1984). "Cytology of the Secretion in Mammalian Sweat Glands". In Bourne, Geoffrey H.; Danielli, James F. (eds.). Protein Diffusion in Cell Membranes: Some Biological Implications. Orlando, Florida: Academic Press. pp. 253–330. ISBN 9780123644879.*

[35] *Baker LB. Sweating Rate and Sweat Sodium Concentration in Athletes: A Review of Methodology and Intra/Interindividual Variability. Sports Med. 2017 Mar;47(Suppl 1):111-128. doi: 10.1007/s40279-017-0691-5. PMID: 28332116; PMCID: PMC5371639.*

[36] *Ogawa, T., Sugenoya, J., Ohnishi, N. et al. Effects of body and head positions on bilateral difference in tympanic temperatures. Eur J Appl Physiol 67, 354–359 (1993). https://doi.org/10.1007/BF00357635*

[37] *Bullard R. W. (1964). EFFECTS OF CARBON DIOXIDE INHALATION ON SWEATING. Journal of applied physiology, 19, 137–141. https://doi.org/10.1152/jappl.1964.19.1.137*

[38] *Sonner, Z., Wilder, E., Heikenfeld, J., Kasting, G., Beyette, F., Swaile, D., Sherman, F., Joyce, J., Hagen, J., Kelley-Loughnane, N., Naik, R. (2015). The microfluidics of the eccrine sweat gland, including biomarker partitioning, transport, and biosensing implications. Biomicrofluidics, 9(3), 031301. https://doi.org/10.1063/1.4921039*

[39] *Moonen, EJM, Haakma, JR, Peri, E, Pelssers, E, Mischi, M, den Toonder, JMJ. Wearable sweat sensing for prolonged, semicontinuous, and nonobtrusive health monitoring. VIEW. 2020; 1:20200077. https://doi.org/10.1002/VIW.20200077*

[40] *Marc Parrilla, Maria Cuartero, Gaston A. Crespo, Wearable potentiometric ion sensors, TrAC Trends in Analytical Chemistry, Volume 110, 2019, Pages 303-320, ISSN 0165-9936, https://doi.org/10.1016/j.trac.2018.11.024. (https://www.sciencedirect.com/science/article/pii/S0165993618303674)*

[41] *Ibrahim, Nur Sabani, Norhayati Johari, Shazlina Manaf, Asrulnizam Abdul Wahab, Asnida Zakaria, Zulkarnay Mohd Noor, Anas. (2022). A Comprehensive Review of the Recent Developments in Wearable Sweat-Sensing Devices. Sensors. 22. 7670. 10.3390/s22197670.*

[42] *Nyein, H.Y.Y.; Tai, L.C.; Ngo, Q.P.; Chao, M.; Zhang, G.B.; Gao, W.; Bariya, M.; Bullock, J.; Kim, H.; Fahad, H.M.; et al. A Wearable Microfluidic Sensing Patch for Dynamic Sweat Secretion Analysis. ACS Sens. 2018, 3, 944–952. [CrossRef] [PubMed]*

[43] *Lee, H.; Song, C.; Hong, Y.S.; Kim, M.S.; Cho, H.R.; Kang, T.; Shin, K.; Choi, S.H.; Hyeon, T.; Kim, D.H. Wearable/disposable sweat-based glucose monitoring device with multistage transdermal drug delivery module. Sci. Adv. 2017, 3, e1601314. [CrossRef] [PubMed]*

[44] *Bandodkar, A.J.; Jia, W.; Yardimci, C.; Wang, X.; Ramirez, J.; Wang, J. Tattoo-based noninvasive glucose monitoring: A proof-of concept study. Anal. Chem. 2015, 87, 394–398. [CrossRef]*

[45] *Ghosh, T.; Chung, H.J.; Rieger, J. All-Solid-State Sodium-Selective Electrode with a Solid Contact of Chitosan/Prussian Blue Nanocomposite. Sensors 2017, 17, 2536. [CrossRef] [PubMed]*

[46] *Zuliani, C.; Matzeu, G.; Diamond, D. A liquid-junction-free reference electrode based on a PEDOT solid-contact and ionogel capping membrane. Talanta 2014, 125, 58–64. [CrossRef]*

[47] *Bariya, M.; Shahpar, Z.; Park, H.; Sun, J.; Jung, Y.; Gao, W.; Nyein, H.Y.Y.; Liaw, T.S.; Tai, L.C.; Ngo, Q.P.; et al. Roll-to-Roll Gravure Printed Electrochemical Sensors for Wearable and Medical Devices. ACS Nano 2018, 12, 6978–6987. [CrossRef]*

[48] *R.Caldwell, "Thermocouple materials," Temperature. Its Measure ment and Control in Science and Industry Reinhold, New York, 1962!, Vol. 3, pp. 81–134*

[49] *P. Bellitti, M. Borghetti, E. Cantù, E. Sardini and M. Serpelloni, "Resistive Sensors for Smart Objects: Analysis on Printing Techniques," in IEEE Transactions on Instrumentation and Measurement, vol. 71, pp. 1-15, 2022, Art no. 9507715, doi: 10.1109/TIM.2022.3181941.*

[50] *P.R.N.Childs, J.R.Greenwood, and C.A. Long , "Review of temperature measurement", Review of Scientific Instruments 71, 2959-2978 (2000) https://doi.org/10.1063/1.1305516*

[51] *Kim, J., Kim, M., Lee, MS. et al. Wearable smart sensor systems integrated on soft contact lenses for wireless ocular diagnostics. Nat Commun 8, 14997 (2017). https://doi.org/10.1038/ncomms14997*

[52] *Pham S, Yeap D, Escalera G, Basu R, Wu X, Kenyon NJ, Hertz-Picciotto I, Ko MJ, Davis CE. Wearable Sensor System to Monitor Physical Activity and the*

Physiological Effects of Heat Exposure. Sensors (Basel). 2020 Feb 6;20(3):855. doi: 10.3390/s20030855. PMID: 32041097; PMCID: PMC7039288.

[53] *Bioelectrical Impedance Spectroscopy for Monitoring Mammalian Cells and Tissues under Different Frequency Domains: A Review Sara Abasi, John R. Aggas, Guillermo G. Garayar-Leyva, Brandon K. Walther, and Anthony Guiseppi-Elie,ACS Measurement Science Au 2022 2 (6), 495-516, DOI: 10.1021/acsmeasuresciau.2c00033*

[54] *Chumlea, W. C., Guo, S. S., Zeller, C. M., Reo, N. V., Siervogel, R. M. (1999). Total body water data for white adults 18 to 64 years of age: the Fels Longitudinal Study. Kidney international, 56(1), 244–252. https://doi.org/10.1046/j.1523-1755.1999.00532.x*

[55] *Claudio A. Téllez-Soto, Michely G. Pereira Silva, Laurita dos Santos, Thiago de O. Mendes, Priyanka Singh, Sabrina A. Fortes, Priscila Favero, Airton A. Martin, In vivo determination of dermal water content in chronological skin aging by confocal Raman spectroscopy, Vibrational Spectroscopy, Volume 112, 2021, 103196, ISSN 0924-2031, https://doi.org/10.1016/j.vibspec.2020.103196.*

[56] *Sempionatto, J.R., Lin, M., Yin, L. et al. An epidermal patch for the simultaneous monitoring of haemodynamic and metabolic biomarkers. Nat Biomed Eng 5, 737–748 (2021). https://doi.org/10.1038/s41551-021-00685-1*